



UNIVERSITI PUTRA MALAYSIA

**SYNTHESIS AND CHARACTERIZATION OF ZINC OXIDE NANORODS
SENSITISED BY Bi_2S_3 , Ag_2S and $\text{Ag}_2\text{S}-\text{Bi}_2\text{S}_3$ FOR
PHOTOELECTROCHEMICAL APPLICATION**

ALZAHHRANI ASLA ABDULLAH M

FS 2020 17



**SYNTHESIS AND CHARACTERIZATION OF ZINC OXIDE NANORODS
SENSITISED BY Bi₂S₃, Ag₂S AND Ag₂S-Bi₂S₃ FOR
PHOTOELECTROCHEMICAL APPLICATION**

ALZAHHRANI ASLA ABDULLAH M



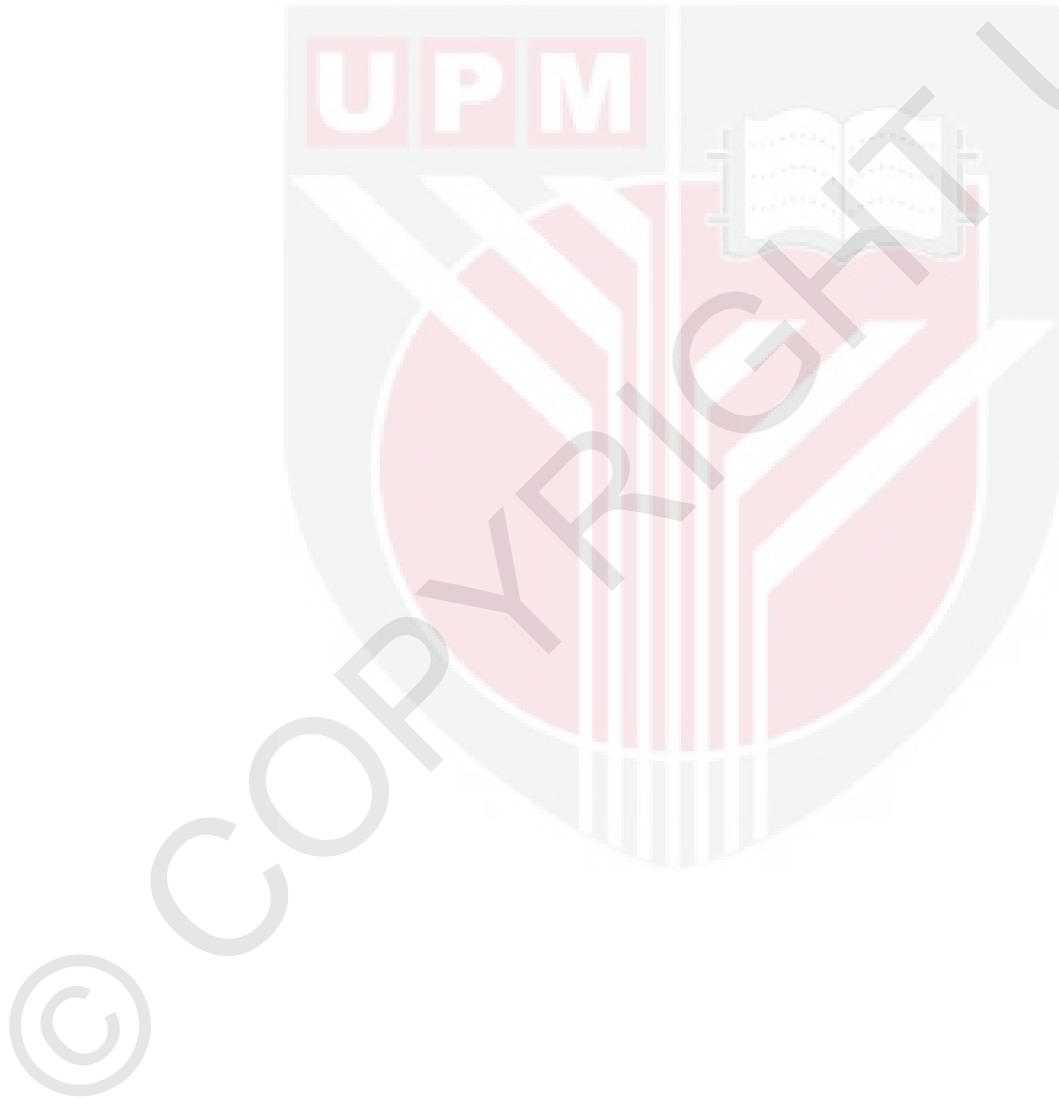
**Thesis Submitted to the School of Graduate Studies, Universiti Putra Malaysia,
in Fulfilment of the Requirements for the Degree of Doctor of Philosophy**

September 2020

COPYRIGHT

All material contained within the thesis, including without limitation text, logos, icons, photographs, and all other artwork, is copyright material of Universiti Putra Malaysia unless otherwise stated. Use may be made of any material contained within the thesis for non-commercial purposes from the copyright holder. Commercial use of material may only be made with the express, prior, written permission of Universiti Putra Malaysia.

Copyright © Universiti Putra Malaysia



DEDICATION

*In appreciation of their love, sacrifices, faith, and endless goodness I
would like to dedicate this thesis to
my dear father may god have mercy on his soul and mother,
my beloved husband, Saleh,
and
our daughters, Lana, Jowana and Nada.*



Abstract of thesis presented to the Senate of Universiti Putra Malaysia in fulfilment
of the requirement for the degree of Doctor of Philosophy

**SYNTHESIS AND CHARACTERIZATION OF ZINC OXIDE NANORODS
SENSITISED BY Bi₂S₃, Ag₂S AND Ag₂S-Bi₂S₃ FOR
PHOTOELECTROCHEMICAL APPLICATION**

By

ALZAHHRANI ASLA ABDULLAH M

September 2020

Chairman : Professor Zulkarnain Zainal, PhD
Faculty : Science

This study focuses on the synthesis and characterisation of zinc oxide nanorods sensitised by narrow bandgap energy metal chalcogenides for photoelectrochemical application. Zinc oxide (ZnO) is a promising oxide semiconductor for photoelectrochemical application. Although it is very efficient in absorbing UV light, its wide bandgap is not ideal for visible light absorption. To solve this problem, heterostructures of the nanocomposite semiconductors such as bismuth sulfide/zinc oxide (Bi₂S₃/ZnO), silver sulfide/zinc oxide (Ag₂S/ZnO) and bismuth sulfide /silver sulfide/ zinc oxide (Bi₂S₃/Ag₂S/ZnO), are proposed to be the alternative conversion medium, as they could possibly harvest larger spectrum of sunlight. There are a variety of modification methods can be applied during the synthesis in order to increase the overall photoconversion efficiency of these nanocomposites such as deposition of sensitised narrow band gap energy materials on the surface of ZnO nanorod arrays. The deposition is expected to result in the modification of the electronic interface and facilitating charge carrier transfer between the coated material and the host semiconductor. In this study, ZnO nanoparticles seed layer (NPs) was prepared by sol-gel spin coating technique followed by heat-treatment at different temperatures to optimise the nucleation. ZnO nanorod arrays (NRAs) were then grown through a simple, facile hydrothermal method. The effect of hydrothermal growth temperature and duration were optimised to ensure achieving the high aspect ratio of ZnO NRAs. Bi₂S₃/ZnO NRAs/ITO, Ag₂S/ZnO NRAs/ITO were prepared using successive ionic layer adsorption and reaction (SILAR) method. In addition, considering the effect of various parameters on formation of Bi₂S₃/ZnO NRAs and Ag₂S/ZnO NRAs nanocomposite, the synthesis was carried out with variation of SILAR cycles number, dipping time, concentration of cationic precursor, pH, and annealing temperature. The formation of ZnO nanorods and Bi₂S₃ was noticed when the colour of the samples changed from colourless to white for ZnO, and dark brown for Bi₂S₃/ZnO. The powder X-ray diffraction (XRD) analysis verified that the synthesised ZnO NRAs sample has

hexagonal phase while Bi_2S_3 has an orthorhombic crystal structure. The deposited photosensitiser has no effect on the host material structure. The small nanoparticles of Bi_2S_3 on ZnO NRAs was observed by field emission scanning electron microscopy (FE-SEM). The red shifted absorbance spectra of the UV-visible spectrophotometry were observed after depositing Bi_2S_3 on ZnO NRAs. On the other hand, the transmission electron microscopy (TEM) provided the estimated average particle size of the Bi_2S_3 /ZnO nanoparticles heterostructure followed by determination of lattice fringe (d-spacing) from high-resolution transmission electron microscopy (HR-TEM). $\text{Bi}_2\text{S}_3/\text{ZnO}$ NRAs nanocomposite synthesised at optimum condition gave a maximum photocurrent density of 2.76 mA/cm^2 and photoconversion efficiency of 3.17% which was 13 times greater than the plain ZnO NRAs (0.25%). The combination of wide bandgap energy (ZnO) with narrow bandgap energy semiconductor caused bending of different Fermi-level positions. Thus, the photogenerated electrons can be transferred easily from conduction band of Bi_2S_3 to the conduction band of ZnO while the holes transferred from the valance band of ZnO NRAs to the valance band of Bi_2S_3 . Furthermore, the formation of ZnO nanorods and Ag_2S was observed as the colour of the samples changed from colourless to white for ZnO NRAs and dark brownish colour for the $\text{Ag}_2\text{S}/\text{ZnO}$ sample. XRD, FE-SEM and UV-visible spectrophotometry analyses showed that the samples synthesised had a monoclinic phase, red shifted on the absorption edge of $\text{Ag}_2\text{S}/\text{ZnO}$ NRAs/ITO. Additionally, ternary nanocomposite thin film $\text{Bi}_2\text{S}_3/\text{Ag}_2\text{S}/\text{ZnO}$ NRAs has been optimised via controlling SILAR cycle number, dipping time, and annealing temperature. Results showed that due to its narrow bandgap, Bi_2S_3 and Ag_2S deposited samples were able to harvest more light compared to plain ZnO NRAs. In comparison with ZnO NRAs/ITO PEC electrode with a bandgap of 3.22 eV, $\text{Bi}_2\text{S}_3/\text{ZnO}$ /ITO and $\text{Ag}_2\text{S}/\text{ZnO}$ /ITO showed much smaller bandgaps of 1.95 eV, 1.78 eV, respectively. This cascading bands gap alignment decreased the chance for electron-hole recombination and enhanced the efficiency of electrons collection. The photoelectrochemical performance of the bare ZnO nanorods, $\text{Bi}_2\text{S}_3/\text{ZnO}$, $\text{Ag}_2\text{S}/\text{ZnO}$ was examined under the illumination of a simulated visible light. The enhancement of photoconversion efficiency was observed to be 3.17% for $\text{Bi}_2\text{S}_3/\text{ZnO}$, 2.33% for $\text{Ag}_2\text{S}/\text{ZnO}$ and 12.63% for $\text{Bi}_2\text{S}_3/\text{Ag}_2\text{S}$ /ZnO compared to plain ZnO nanorods sample of only 0.25%.

Abstrak tesis yang dikemukakan kepada Senat Universiti Putra Malaysia sebagai memenuhi keperluan untuk ijazah Doktor Falsafah

**SINTESIS DAN PENCIRIAN ROD NANO ZINK OKSIDA DIPEKA OLEH
 Bi_2S_3 , Ag_2S DAN $\text{Ag}_2\text{S}\text{-}\text{Bi}_2\text{S}_3$ UNTUK APLIKASI FOTOELEKTROKIMIA**

Oleh

ALZAHHRANI ASLA ABDULLAH M

September 2020

Pengerusi : Profesor Zulkarnain bin Zainal, PhD
Fakulti : Sains

Kajian ini memberi tumpuan kepada sintesis dan pencirian rod nano zink oksida yang dipeka oleh logam kalkogenida berluang tenaga sempit untuk aplikasi fotoelektrokimia. Zink oksida (ZnO) adalah semikonduktor oksida yang berpotensi untuk aplikasi fotoelektrokimia. Walaupun sangat berkesan untuk menyerap cahaya UV, luang tenaganya yang besar adalah tidak sesuai untuk penyerapan cahaya nampak. Untuk menyelesaikan masalah ini, semikonduktor komposit nano heterostruktur seperti bismut sulfida/zink oksida ($\text{Bi}_2\text{S}_3/\text{ZnO}$), argentum sulfida/zink oksida ($\text{Ag}_2\text{S}/\text{ZnO}$) dan bismut sulfida/argentum sulfida/zink oksida, ($\text{Bi}_2\text{S}_3/\text{Ag}_2\text{S}/\text{ZnO}$) dicadangkan sebagai medium penukaran alternatif kerana berpotensi menyerap spektrum solar pada julat yang lebih besar. Terdapat pelbagai cara pengubahsuaian yang boleh digunakan semasa proses sintesis bagi memastikan kecekapan keseluruhan penukaran tenaga cahaya komposit nano ini dapat ditingkatkan seperti pemendapan bahan luang tenaga sempit terpeka pada permukaan barisan rod nano ZnO . Pengenapan ini dijangka menghasilkan pengubahsuaian antara muka elektronik dan membantu pemindahan pembawa cas antara bahan enapan dan semikonduktor hos. Dalam kajian ini, lapisan benih partikel nano ZnO (NPs) disediakan melalui teknik salutan berputar sol-gel diikuti oleh rawatan haba pada suhu yang berbeza untuk mengoptimumkan penukleusan. Barisan rod nano ZnO kemudiannya ditumbuhkan melalui kaedah hidroterma yang mudah dan ringkas. Kesan suhu dan tempoh pertumbuhan hidroterma dioptimumkan untuk mendapatkan nisbah aspek ZnO NRAs yang tinggi. $\text{Bi}_2\text{S}_3/\text{ZnO}$ NRAs/ITO, $\text{Ag}_2\text{S}/\text{ZnO}$ NRAs /ITO telah disediakan menggunakan kaedah penjerapan dan tindak balas lapisan ionik berturut (SILAR). Tambahan itu, dengan mengandaikan kesan pelbagai parameter ke atas pembentukan komposit nano $\text{Bi}_2\text{S}_3/\text{ZnO}$ dan $\text{Ag}_2\text{S}/\text{ZnO}$ NRAs /ITO, sintesis telah dijalankan dengan variasi bilangan kitaran SILAR, masa pencelupan, kepekatan prekursor kationik, pH, dan suhu penyepuhlindapan. Pembentukan rod nano ZnO dan Bi_2S_3 dapat dikesan apabila warna sampel berubah daripada tidak berwarna kepada putih untuk ZnO , dan coklat gelap untuk $\text{Bi}_2\text{S}_3/\text{ZnO}$. Analisis pembelauan X-ray

(XRD) mengesahkan bahawa sampel ZnO NRAs yang disintesis mempunyai fasa heksagonal manakala Bi₂S₃ mempunyai struktur kristal ortorombik. Pemakaian tenaga cahaya yang dienapkan tidak memberi kesan terhadap struktur bahan hos. Struktur partikel nano Bi₂S₃ yang kecil di atas ZnO NRAs telah diperhatikan melalui mikroskopi pengimbasan elektron pancaran medan (FE-SEM). Peralihan merah spektrum penyerapan dapat diperhatikan daripada spektrum UV-nampak selepas pengenapan Bi₂S₃ pada ZnO NRAs. Sementara itu, mikroskopi transmisi elektron (TEM) memberi anggaran purata saiz partikel Bi₂S₃/ZnO heterostruktur diikuti penentuan jarak pinggiran kekisi (d-spacing) daripada mikroskopi transmisi elektron beresolusi tinggi (HR-TEM). Komposit nano Bi₂S₃/ZnO NRA yang disintesis pada keadaan optimum memberikan ketumpatan arus tenaga cahaya maksimum pada 2.76 mA/cm² dan kecekapan penukaran tenaga cahaya sebanyak 3.17% iaitu 13 kali lebih baik daripada ZnO NRAs kosong (0.25%). Gabungan semikonduktor ZnO berluang tenaga luas dengan semikonduktor berluang tenaga sempit telah menhasilkan lenturan posisi aras Fermi yang berlainan. Oleh itu, elektron terjana tenaga cahaya dapat dipindahkan dengan mudah daripada jalur konduksi Bi₂S₃ ke jalur konduksi ZnO sementara lubang dipindahkan dari jalur valensi ZnO NRAs ke jalur valensi Bi₂S₃. Seterusnya, pembentukan rod nano ZnO dan Ag₂S diperhatikan apabila warna sampel berubah daripada tidak berwarna kepada putih untuk ZnO NRAs dan warna coklat gelap untuk sampel Ag₂S/ZnO. Analisis XRD, FE-SEM dan spektrofotometri UV-nampak menunjukkan sampel yang disintesis mempunyai fasa monoklinik, dan teralih merah pada hujung penyerapan bagi Ag₂S/ZnO NRAs/ITO. Sebagai tambahan, filem nipis komposit nano ternari Bi₂S₃/Ag₂S/ZnO NRAs telah dioptimumkan melalui kawalan bilangan kitaran SILAR, masa pencelupan dan suhu penyepuhlindapan. Keputusan mendapati luang tenaga yang sempit menyebabkan sampel yang dienapkan Bi₂S₃ dan Ag₂S dapat menyerap lebih banyak cahaya berbanding dengan ZnO NRAs kosong. Sebagai perbandingan dengan elektrod PEC ZnO NRAs/ITO berluang tenaga 3.22 eV, Bi₂S₃/ZnO/ITO dan Ag₂S/ZnO/ITO menunjukkan luang tenaga yang lebih kecil iaitu masing-masing 1.95 eV dan 1.78 eV. Penurunan berurutan luang jalur ini mengurangkan peluang untuk penggabungan semula elektron-lubang dan meningkatkan kecekapan pengumpulan elektron. Prestasi fotolektrokimia rod nano ZnO, Bi₂S₃/ZnO, Ag₂S/ZnO diperhatikan di bawah sinaran cahaya nampak simulasi. Peningkatan kecekapan penukaran tenaga cahaya yang diperhatikan ialah 3.17% untuk Bi₂S₃/ZnO, 2.33% untuk Ag₂S/ZnO dan 12.63% untuk Bi₂S₃/Ag₂S/ZnO berbanding rod nano ZnO dengan hanya 0.25%.

ACKNOWLEDGEMENTS

This thesis would never have existed without Allah's blessings. I would like to thank Allah the Almighty for giving me the strength, patience, and motivation to complete my PhD thesis despite the many challenges that I faced. Furthermore, without the supervision, guidance, encouragement, and help provided by the individuals listed below, the successful completion of his thesis would not have been possible. Therefore, it is with heartfelt gratitude that I extend my sincere appreciation to the following individuals: first of all, I would like to express my sincere thanks to my supervisor, Professor Dr. Zulkarnain, for his supervision, encouragement, and support during the whole PhD study period. His meticulous attention to detail, his insightful and informative feedback and his thoughtful comments helped me frame the direction of this thesis in the appropriately required form. His commitment and enthusiasm for scientific research, his obvious wealth and depth of knowledge were obvious and played a crucial role in guiding me continuing scientific progress. Ultimately, his constant input of time, patience and moral support has been critical in helping me to successfully complete this challenging to accomplish my academic journey.

My greatest appreciation is also extended to my co-supervisors, Professor Dr. Zainal Abidin Talib, Associate Professor Dr. Hong-Ngee Lim for their guidance, supportive advice, and estimated comments. Their vast knowledge, experience and tireless assistance have helped me through the more difficult parts of data analysis.

It is also my pleasure to thank Dr. Araa Mebdir Holi who contributed substantially to my effort in laying down the technical foundation of the work presented here, and who gave me great support during each stage of my doctoral study. Much of this work would not never be satisfactorily completed without her valuable assistance.

I also deeply appreciate my parents, and even though we have been half a world apart during the years of my study, I have always been able to feel their unconditional love and support. My thanks go to my beloved husband, Saleh, our daughters, Lana, Jowana and Nada. Their love, patience, sacrifices, and encouragement light up many lonely moments in my life as a postgraduate student away from home and have given me strength and courage when I was down.

I would like to express my sincere thanks to all my friends, especially my close friend Mahaniem, for her help and the interesting scientific discussions with her during my research and the colleagues in the research group, Dr. Nazihah, Laimy, Eydar, Mozaker, Tan and Aqila. Their support, friendship and encouragement made my PhD study a happy journey.

Special thanks are also due to the Department of Chemistry and Department of Physics, Faculty of Science, Universiti Putra Malaysia, and the Microscopy Unit, Institute of Bioscience, and Mimos Berhad. I would also like to acknowledge with thanks the assistance of the Saudi Cultural Mission and Imam Abdul Rahman Bin Faisal University for the financial support via a scholarship. Furthermore, I am grateful to every individual who has helped me in one way or another during the journey of my PhD study. May Allah bless you all.



This thesis was submitted to the Senate of the Universiti Putra Malaysia and has been accepted as fulfilment of the requirement for the degree of Doctor of Philosophy. The members of the Supervisory Committee were as follows:

Zulkarnain Zainal, PhD

Professor

Faculty of Science

Universiti Putra Malaysia

(Chairman)

Zainal Abidin Talib, PhD

Professor

Faculty of Science

Universiti Putra Malaysia

(Member)

Hong-Ngee Lim, PhD

Professor

Faculty of Science

Universiti Putra Malaysia

(Member)

ZALILAH MOHD SHARIFF, PhD

Professor and Dean

School of Graduate Studies

Universiti Putra Malaysia

Date: 12 November 2020

TABLE OF CONTENTS

	Page
ABSTRACT	i
ABSTRAK	iii
ACKNOWLEDGEMENTS	v
APPROVAL	vii
DECLARATION	ix
LIST OF TABLES	xiv
LIST OF FIGURES	xvi
LIST OF ABBREVIATIONS	xxviii
 CHAPTER	
1 INTRODUCTION	1
1.1 Background of the Study	1
1.2 Problem Statement	3
1.3 Study Objectives	4
1.4 Significance of the Study	5
1.5 Scope of the Study	5
2 LITERATURE REVIEW	7
2.1 Introduction	7
2.2 Properties of nanomaterials	8
2.2.1 One-dimensional Metal-oxide Nanostructures	8
2.2.2 Heterostructured-semiconductor	9
2.3 Photoelectrochemical cell	11
2.3.1 Fundamental principles of photoelectrochemical cells	12
2.3.2 The Quantum Confinement Theory in nano scaled semiconductor	16
2.4 Properties of zinc oxide (ZnO)	18
2.5 Approaches in synthesising zinc oxide thin film	20
2.6 Synthesis of ZnO nanorod arrays	22
2.6.1 Vapour phase deposition	23
2.6.2 Metal organic chemical vapour deposition (MOCVD)	23
2.6.3 Chemical bath deposition (CBD)	24
2.6.4 Pulse laser deposition (PLD)	24
2.6.5 Electrodeposition (ED)	25
2.6.6 Hydrothermal Method (HT)	25
2.7 Synthesis methods of sensitised semiconductors	27
2.8 Bismuth sulfide properties	31
2.9 Previous works on Bi ₂ S ₃ /metal oxide semiconductor	32
2.10 Silver sulphide properties	37
2.11 Previous work on Ag ₂ S/ metal oxide semiconductor	38
2.12 Previous work on Bi ₂ S ₃ /Ag ₂ S	40

3	METHODOLOGY	43
3.1	Introduction	43
3.2	Synthesis methods	43
3.3	Chemical reagents	45
3.4	Preparation of ZnO nanoparticles via sol-gel spin coating technique	45
3.5	Preparation of ZnO nanorod arrays (NRAs) using hydrothermal method (HT)	46
3.6	Preparation of Bi ₂ S ₃ /ZnO NRAs nanocomposites via (SILAR) method	47
3.7	Preparation of Ag ₂ S/ZnO NRAs nanocomposites via (SILAR) method	48
3.8	Fabrication of Bi ₂ S ₃ / Ag ₂ S/ZnO NRAs nanocomposites via SILAR method	49
3.9	Characterisation techniques	50
3.9.1	Ultraviolet-visible (UV-Vis) spectroscopy	50
3.9.2	Powder X-ray diffraction (XRD)	51
3.9.3	Raman spectroscopy	53
3.9.4	Field emission scanning electron microscopy (FE-SEM) analysis	53
3.9.5	Transmission electron microscopy (TEM)	54
3.9.6	Energy dispersive X-ray spectroscopy	55
3.9.7	X-ray photoelectron spectroscopy (XPS)	55
3.9.8	Photoelectrochemical performance (PEC)	56
4	ZnO NANOSTRUCTURES LAYER	60
4.1	Introduction	60
4.2	Sol-gel spin coating deposition of ZnO nanoparticles (NPs) seed layer	60
4.3	Hydrothermal growth of ZnO nanorod arrays (NRAs)	66
4.3.1	Effect of growth temperature on ZnO NRAs	67
4.3.2	Effect of growth time on ZnO NRAs	76
5	SYNTHESIS AND CHARACTERIZATION OF Bi₂S₃/ZnO NRAs FOR PHOTOELECTROCHEMICAL APPLICATION	85
5.1	Introduction	85
5.2	Effect of varying SILAR cycles number	85
5.3	Effect of SILAR dipping time	91
5.4	Effect of varying cationic concentration	96
5.5	Effect of varying pH of cationic precursor	102
5.6	Effect of annealing temperature	107
6	SYNTHESIS AND CHARACTERIZATION OF Ag₂S/ZnO NRAs FOR PHOTOELECTROCHEMICAL APPLICATION	122
6.1	Introduction	122
6.2	Effect of varying SILAR cycle number	122
6.3	Effect of SILAR dipping time	128
6.4	Effect of varying cationic concentration	134
6.5	Effect of varying pH of cationic precursor	138

6.6	Effect of annealing temperature	143
7	SYNTHESIS AND CHARACTERIZATION OF Bi₂S₃/Ag₂S/ ZnO NRAs FOR PHOTOLELECTROCHEMICAL APPLICATION	156
7.1	Introduction	156
7.2	Effect of SILAR cycles	156
7.3	Effect of dipping time	161
7.4	Effect of varying annealing temperature	166
7.5	Comparison between ZnO NRAs, Bi ₂ S ₃ /ZnO NRAs, Ag ₂ S/ ZnO NRAs and Bi ₂ S ₃ /Ag ₂ S /ZnO NRAs/ITO	176
8	CONCLUSIONS	188
8.1	Conclusions	188
8.2	Recommendations for future work	190
REFERENCES		191
APPENDICES		209
BIODATA OF STUDENT		222
LIST OF PUBLICATIONS		223

LIST OF TABLES

Table	Page
2.1 Classification of quantum confined structures	17
2.2 Overview on $\text{Bi}_2\text{S}_3/\text{ZnO}$ and $\text{Ag}_2\text{S}/\text{ZnO}$ thin films used for photoelectrochemical cells	42
3.1 Chemicals materials and solvents used throughout this work	45
3.2 Parameters studied in $\text{Bi}_2\text{S}_3/\text{ZnO}/\text{ITO}$ via SILAR method	48
3.3 Parameters studied in $\text{Ag}_2\text{S}/\text{ZnO}/\text{ITO}$ via SILAR method	49
3.4 Parameters studied in $\text{Bi}_2\text{S}_3/\text{Ag}_2\text{S}/\text{ZnO}$ NRAs/ITO	49
3.5 Compounds and their JCPDS reference codes	52
4.1 The particle size values of ZnO NPs seed layer at various annealing temperatures	62
4.2 Values of photo conversion efficiency ($\eta\%$) of ZnO NPs seed layer at different annealing temperatures	66
4.3 Summarised data depicting the XRD patterns of aligned ZnO NRAs/ITO	68
4.4 Summarised data of the FE-SEM images (thickness, diameter, and aspect ratio), E_g values, and photocurrent density of aligned ZnO NRAs/ ITO	71
4.5 Summarised data from FE-SEM images of ZnO/ITO NRAs at 110 °C for different growth time	77
4.6 Comparative study for synthesised ZnO NRAs /ITO at different hydrothermal growth temperature, growth time and different methods for seed layer fabrication	84
5.1 Photocurrent density and photoconversion efficiency values of $\text{Bi}_2\text{S}_3/\text{ZnO}$ NRAs at different cationic concentration	100
5.2 The calculated C.B. and V.B. position values of various constructions of nanostructure	121
6.1 The photoelectrochemical conversion efficiency of $\text{Ag}_2\text{S}/\text{ZnO}$ NRAs/ ITO at different dipping time	134
6.2 The conduction band and valance band position of $\text{Ag}_2\text{S}/\text{ZnO}$ NRAs at different annealing temperatures	155

7.1	EDS data of Bi ₂ S ₃ /ZnO/ITO; Ag ₂ S/ZnO/ITO; and Bi ₂ S ₃ /Ag ₂ S/ZnO /ITO	181
7.2	Comparison of binding energy of Bi ₂ S ₃ /ZnO, Ag ₂ S/ZnO and Bi ₂ S ₃ /Ag ₂ S/ZnO	182
7.3	Comparison of optical properties calculated C.B. and V.B. positions of bare ZnO NRAs/ITO, Bi ₂ S ₃ /ZnO NRAs/ITO, Ag ₂ S/ZnO NRAs/ITO, and Bi ₂ S ₃ /Ag ₂ S /ZnO NRAs/ITO	184



LIST OF FIGURES

Figure	Page
2.1 Diagram illustrates the heterostructured-alignment process in which C. B and V.B. symbolise the valence band and conduction band, respectively. (a) Type I band alignment: "Straddling" ; (b) Type II staggered gap and (c) Type III broken gap	10
2.2 Energy band diagram for a n-type semiconductor (a) before contact; (b) after dark-equilibration; (c) illuminated-equilibration of Fermi levels at the semiconductor/ electrolyte interface and presence of band-bending and space charged layer (SCL)	14
2.3 Density of states presented in different confinement configurations	17
2.4 Demonstration of ZnO crystal structures: (a) cubic rock salt, (b) cubic zinc blend and (c) hexagonal wurtzite structure. The colored blue and yellow spheres symbolise zinc and oxygen atoms, respectively (Özgür et al., 2018)	19
2.5 ZnO's typical wurtzite crystal structure (Rodnyi & Khodyuk, 2011)	19
2.6 Schematic diagram of methods which are used in ZnO thin film synthesis	20
2.7 Sol-gel coating methods: (a) dip-coating and (b) spin-coating	22
2.8 Schematic diagram deposition SILAR growth. (i) adsorption of precursor K _L p on the substrate surface and the formation of the electrical double layer; (ii) rinsing step; (iii) reaction of K _L p surface species with the precursor A _L q and (iv) rinsing(II)	30
2.9 Schematic drawing of the orthorhombic crystal structure of Bi ₂ S ₃	32
2.10 Diagrammatic illustrations of (i) monoclinic acantite (α -Ag ₂ S); (ii) cubic argentite (β -Ag ₂ S) structure	38
3.1 Schematic diagram of research flowchart	44
3.2 Schematic diagram of the preparation of ZnO NPs seed layer by sol - gel spin coating	46
3.3 Schematic diagram of the preparation of ZnO NRAs by hydrothermal method	47
3.4 Diagram of preparation Bi ₂ S ₃ /ZnO NRAs nanoparticles via SILAR method of cationic and anionic precursor (\bullet =Bi ³⁺ and \bullet =S ²⁻)	48
3.5 The schematic diagram of X-ray diffraction	52

3.6	Set-up for photoelectrochemical experiments	58
4.1	Field emission scanning electron microscopy (FE-SEM) images of ZnO NPs (seed layer) with two different magnifications ($\times 50,000$ and $\times 100,000$) annealed at different temperatures of (a) 300 °C; (b) 350 °C; (c) 400 °C; (d) 450 °C	61
4.2	X-ray diffractogram of ZnO NPs at different annealing temperatures of: (a) plain ITO; (b) 300 °C; (c) 350 °C; (d) 400 °C; and (e) 450 °C	63
4.3	The absorbance spectra of ZnO NPs at the different annealing temperatures of: (a) 300 °C; (b) 350 °C; (c) 400 °C; and (d) 450 °C	63
4.4	Bandgap energy curves of ZnO NPs at the different annealing temperatures of: (a) 300 °C; (b) 350 °C; (c) 400 °C; and (d) 450 °C	64
4.5	Linear sweep voltammograms of ZnO/ITO NPs (seed layers) prepared at the different annealing temperatures at scan rate of 20 mV/s from -0.5 V to +1.0 V: (a) 300 °C; (b) 350 °C; (c) 400 °C; (d) 450 °C	65
4.6	The graph of photocurrent density (J_{ph}) at +0.5 V applied voltage vs. Ag/AgCl plotted against the annealing temperature of ZnO/ITO NPs (seed layers)	66
4.7	X-ray diffraction of ZnO NRAs/ITO at different hydrothermal growth temperatures for 4 hours (a) ITO substrate; (b) 80 °C; (c) 90 °C; (d) 100 °C; (e) 110 °C and (f) 120 °C. The inset of figure represents the (002) peak plotted from 34° to 35.5°	68
4.8	Top view and cross section FE-SEM images of ZnO NRAs/ITO grown for 4 hours at different hydrothermal temperatures: (a) 80 °C; (b) 90 °C; (c) 100 °C; (d) 110 °C; and (e) 120 °C	70
4.9	ZnO NRAs growth temperature vs. change in length, diameter, and aspect ratio (insets)	72
4.10	The absorbance spectra of ZnO NRAs/ITO grown for 4 hours at different hydrothermal temperatures: (a) 80 °C; (b) 90 °C; (c) 100 °C; (d) 110 °C and (e) 120 °C	73
4.11	The Tauc plot $(\alpha h\nu)^2$ versus energy ($h\nu$) of ZnO NRAs/ITO grown for 4 hours at different hydrothermal temperatures: (a) 80 °C; (b) 90 °C; (c) 100 °C; (d) 110 °C and (e) 120 °C	74
4.12	Linear sweep voltammograms of (a) ZnO NPs (seed layer); ZnO NRAs /ITO synthesised at different hydrothermal temperatures (b) 80 °C; (c) 90 °C; (d) 100 °C; (e) 110 °C and (f) 120 °C for 4 hours obtained at the scan rate of 20 mVs ⁻¹ at the applied potentials from -0.5 V to +1.0 V under illumination intensity of 100 mWcm ⁻² in 0.1 M Na ₂ S and 0.1 M Na ₂ SO ₃ electrolyte	75

4.13	Photocurrent density (J_{ph}) (mA/cm^2) plotted against growth temperature ($^\circ\text{C}$) at applied potential of +0.5V vs. Ag/AgCl	76
4.14	X-ray diffractograms of ZnO NRAs prepared at 110 $^\circ\text{C}$ using hydrothermal method at different growth times: (a) ITO substrate; (b) 1h;(c) 2h; (d) 3h; (e) 4h; and (f) 5h. The inset of figure represents the (002) peak plotted from 34 $^\circ$ to 35 $^\circ$	77
4.15	Top view and cross section FE-SEM images of ZnO NRAs/ITO grown at 110 $^\circ\text{C}$ for different growth time: (a) 1h; (b) 2h; (c) 3h; (d) 4h; and (e) 5h	78
4.16	The absorbance spectra of ZnO NRAs/ITO grown at 110 $^\circ\text{C}$ via hydrothermal method at different growth time: (a) 1h;(b) 2h; (c) 3h; (d) 4h; and (e) 5h	79
4.17	The Tauc plot $(\alpha h\nu)^2$ versus energy ($h\nu$) ZnO NRAs/ITO grown at 110 $^\circ\text{C}$ via hydrothermal method at different growth time: (a) 1h;(b) 2h; (c) 3h; (d) 4h; and (e) 5h	80
4.18	Graph of optical bandgap energy of ZnO NRAs prepared via hydrothermal method at 110 $^\circ\text{C}$ against the growth time	81
4.19	Linear sweep voltammograms of: (a) ZnO NPs (seed layer); ZnO NRAs/ITO synthesised at 110 $^\circ\text{C}$ using hydrothermal method at different growth time: (b) 1h;(c) 2h; (d) 3h; (e) 4h; and (f) 5h obtained at the scan rate of 20 mVs^{-1} at the applied potentials from -0.5 V to 1.0 V under illumination intensity of 100 mWcm^{-2} in 0.1 M Na ₂ S and 0.1 M Na ₂ SO ₃ electrolyte	82
4.20	Photo conversion efficiency values ZnO NRAs/ITO synthesised at 110 $^\circ\text{C}$ using hydrothermal method at different growth time: (a) 1h;(b) 2h; (c) 3h; (d) 4h; and (e) 5h under illumination intensity of 100 mWcm^{-2} in 0.1M Na ₂ S and 0.1M Na ₂ SO ₃ electrolyte system	83
5.1	X-ray diffraction of: (a) ZnO NRAs, Bi ₂ S ₃ /ZnO NRAs/ITO at different SILAR cycles of (b) 3 cycles; (c) 5 cycles; (d) 7 cycles; (e) 9 cycles; (f) 11 cycles	86
5.2	(A) UV-Vis Spectra; (B) bandgap energy curves of: (a) ZnO NRAs/ITO and Bi ₂ S ₃ /ZnO NRAs/ITO prepared at different SILAR cycles (b) 3 cycles; (c) 5 cycles; (d) 7 cycles ;(e) 9 cycles; (f) 11 cycles and the inset plot shows the optical band gap energy at different SILAR cycles	87
5.3	Different magnification($\times 25,000$ and $\times 50,000$) FE-SEM images of (a) pristine ZnO NRAs and ZnO nanorods decorated with Bi ₂ S ₃ nanoparticles for (b) 3 cycles; (c) 7 cycles; (d) 11 cycles. Cross-sectionals of the samples a, c is shown in the insets of the figures	88

5.4	Energy dispersive X-ray (EDX) spectra of Bi ₂ S ₃ /ZnO NRAs/ITO heterostructure at (a) 3 cycles; (b) 7 cycles of Bi ₂ S ₃ /ZnO NRAs/ITO heterostructure. Inset shows the tabulated EDX data in atomic% of the corresponding films	89
5.5	Linear sweep voltammograms obtained at the scan rate of 20 mV s ⁻¹ at applied potentials from -0.5V to +1.0 V under illumination intensity of 100 mWcm ⁻² in 0.1M Na ₂ S and Na ₂ SO ₃ electrolyte for: (a) bare ZnO NRAs/ITO; Bi ₂ S ₃ /ZnO NRAs/ITO at different SILAR cycles number: (b) 3 cycles; (c) 5 cycles; (d) 7 cycles; (e) 9 cycles; (f) 11 cycles	90
5.6	Photoconversion efficiency as a function of applied voltage versus (Ag/AgCl) of: (a) bare ZnO NRAs/ITO; (b) Bi ₂ S ₃ /ZnO NRAs prepared at 7 SILAR cycles under illumination intensity of 100 mWcm ⁻² in 0.1M Na ₂ SO ₃ and 0.1M Na ₂ S electrolyte mixture	91
5.7	FE-SEM images of: (a) ZnO NRAs/ITO and Bi ₂ S ₃ /ZnO NRAs/ITO prepared at different dipping time (b) 20 s;(c) 60 s; (d) 100 s Cross sectional images of (a) and (c) are shown in insets of the figures	92
5.8	X-ray diffraction of: (a) ZnO NRAs; Bi ₂ S ₃ /ZnO NRAs/ITO at different dipping time of (b) 20 s; (c) 40 s; (d) 60 s; (e) 80 s; (f) 100 s	93
5.9	(A) UV-Vis Spectra; (B) bandgap energy curves of: (a) ZnO NRAs/ ITO and Bi ₂ S ₃ /ZnO NRAs/ITO prepared at different dipping time (b) 20 s;(c) 40 s; (d) 60 s ;(e) 80 s; (f) 100 s and the inset plot shows the optical band gap energy values at different dipping time	94
5.10	Linear sweep voltammograms obtained at the scan rate of 20 mV s ⁻¹ at applied potentials from -0.5V to +1.0 V under illumination intensity of 100 mWcm ⁻² in 0.1M Na ₂ S and Na ₂ SO ₃ electrolyte for: (a) bare ZnO NRAs/ITO; Bi ₂ S ₃ /ZnO NRAs/ITO at different dipping time (b) 20 s; (c) 40 s; (d) 60 s ;(e) 80 s; (f) 100 s	95
5.11	Photoconversion efficiency as a function of applied voltage versus (Ag/AgCl) of Bi ₂ S ₃ /ZnO NRAs prepared with different dipping time: (a) 20 s;(b) 40 s; (c) 60 s ;(d) 80 s; (e) 100 s under illumination intensity of 100 mWcm ⁻² in 0.1M Na ₂ SO ₃ and 0.1M Na ₂ S electrolyte mixture	96
5.12	X-ray diffraction of: (a) ZnO NRAs ; Bi ₂ S ₃ /ZnO NRAs/ITO at different cationic concentration of (b) 1 mM;(c) 3 mM; (d) 5 mM; (e) 8 mM; (f) 10 mM	97
5.13	FE-SEM images of (a) bare ZnO NRAs, ZnO NRAs decorated with Bi ₂ S ₃ nanoparticles at different cationic concentration (b) 1 mM; (c) 3 mM; (d) 10 mM. Cross-sectional images of bare ZnO NRAs (a), higher magnification (\times 50,000) of (b),(c),(d) is shown in the insets of the figures	98

5.14	(A) UV-Vis spectra; (B) the bandgap energy curves of: (a) ZnO NRAs /ITO and Bi ₂ S ₃ /ZnO NRAs/ITO prepared at different cationic concentration (b) 1 mM;(c) 3 mM ;(d) 5 mM ;(e) 8 mM; (f) 10 mM. The optical band gap energy values at different cationic concentrations is shown in the insets of figure	99
5.15	Linear sweep voltammograms obtained at the scan rate of 20 mV s ⁻¹ at applied potentials from -0.5 V to +1.0 V under illumination intensity of 100 mWcm ⁻² in 0.1M Na ₂ S and Na ₂ SO ₃ electrolyte for: (a) bare ZnO NRAs/ITO; Bi ₂ S ₃ /ZnO NRAs/ITO at different cationic concentration : (b) 1 mM; (c) 3 mM; (d) 5 mM; (e) 8 mM; (f) 10 mM	101
5.16	Photoconversion efficiency values as a function of applied voltage vs. Ag/AgCl of Bi ₂ S ₃ /ZnO NRAs at different cationic concentration: (a) 1mM; (b) 3mM; (c) 5 mM; (d) 8 Mm; (e) 10 mM, under illumination intensity (100 mW cm ⁻²) in 0.1 M Na ₂ S and 0.1 M Na ₂ SO ₃	102
5.17	X-ray diffraction patterns of: (a) ZnO NRAs; Bi ₂ S ₃ /ZnO NRAs/ITO with different pH cationic precursor: (b) 1.3;(c) 2.3; (d) 3.3; (e) 4.3; (f) 5.3	103
5.18	FE-SEM images of: ZnO NRAs (a) ;Bi ₂ S ₃ /ZnO NRAs/ITO with different cationic pH: (b) 1.3; (c) 2.3; (d) 3.3; (e) 4.3; (f) 5.3	104
5.19	(A) UV-Vis spectra and (B) the optical bandgap Eg energy curves of: (a) ZnO NRAs/ITO and Bi ₂ S ₃ /ZnO NRAs/ITO prepared at different pH cationic (b) 1.3; (c) 2.3 ;(d) 3.3 ;(e) 4.3; (f) 5.3. The optical band gap energy values at different cationic pH is shown in the insets of figure	105
5.20	Linear sweep voltammograms obtained at the scan rate of 20 mVs ⁻¹ at applied potentials from -0.5 V to +1.0 V under illumination intensity of 100 mWcm ⁻² in 0.1M Na ₂ S and Na ₂ SO ₃ electrolyte for: (a) bare ZnO NRAs/ITO; Bi ₂ S ₃ /ZnO NRAs/ITO at different cationic pH: (b) 1.3; (c) 2.3; (d) 3.3; (e) 4.3; (f) 5.3	106
5.21	Photoconversion efficiency values of (a) ZnO NRAs/ITO; Bi ₂ S ₃ /ZnO NRAs/ITO as a function of applied voltage vs. Ag/AgCl of at different pH cationic: (b) 1.3; (c) 2.3; (d) 3.3; (e) 4.3; (f) 5.3 under illumination intensity (100 mW cm ⁻²) in 0.1 M Na ₂ S and 0.1 M Na ₂ SO ₃	107
5.22	X-ray diffraction of: (a) ZnO NRAs/ITO; Bi ₂ S ₃ /ZnO NRAs/ITO at various annealing temperatures: (b) as deposited, (c) 100 °C; (d) 200 °C; (e) 300 °C; (f) 400 °C; (g) 500 °C. The inset of figure represents the peaks plotted from 2θ 25°to 33°	108
5.23	Raman spectra of (a) ZnO NRAs; (b) Bi ₂ S ₃ /ZnO NRAs annealed at 300 °C for 1h in N ₂ gas flow	109

5.24	XPS spectra of Bi ₂ S ₃ /ZnO/ITO heterostructure annealed at 300 °C: (a) the overall spectra Bi ₂ S ₃ /ZnO/ITO; (b) Bi 4f and S 2p spectra; (c) O 1s spectra and (d) Zn 2p spectra	110
5.25	(A) UV-Vis spectra; (B) the optical bandgap energy curves of: (a) ZnO NRAs/ITO; (b) Bi ₂ S ₃ /ZnO NRAs/ITO as-deposited and Bi ₂ S ₃ /ZnO NRAs/ITO annealed at (c) 100 °C;(d) 200 °C ;(e) 300 °C ;(f) 400 °C; (g) 500 °C	111
5.26	FE-SEM images at two different magnification ($\times 25,000$ and $\times 50,000$) of: (a) ZnO NRAs, (b) as-prepared Bi ₂ S ₃ /ZnO NRAs, Bi ₂ S ₃ /ZnO NRAs at different annealing temperatures (c) 200 °C; (d) 300 °C; (e) 400 °C. (f) 500 °C. Cross sectional images of (a) and (d) are shown in the insets of the figures	113
5.27	(a) The SAED pattern of plain ZnO NRAs; (b) The SAED pattern of Bi ₂ S ₃ /ZnO NRAs annealed at 300 °C for 1 h in N ₂ flow; (c) TEM image of plain ZnO NRAs; (d) TEM image of the optimal sample Bi ₂ S ₃ /ZnO NRAs annealed at 300 °C for 1 h in N ₂ flow	114
5.28	FFT patterns for Bi ₂ S ₃ /ZnO obtained from the selected area in HRTEM image under 5 nm scale	115
5.29	The EDS pattern and elemental mapping (EELS) of the optimum sample Bi ₂ S ₃ /ZnO NRAs/ITO annealed at 300 °C for 1h under N ₂ air flow	116
5.30	Linear sweep voltammograms of (a) as-deposited Bi ₂ S ₃ /ZnO NRAs, and Bi ₂ S ₃ /ZnO NRAs annealed at (b) 100 °C; (c) 200 °C; (d) 300 °C; (e) 400 °C; (f) 500 °C for 1h, obtained at the scan rate of 20 mVs ⁻¹ at the applied potential from -0.5V to +1.0 V under illumination intensity (100 mW cm ⁻²) in 0.1 M of Na ₂ S and 0.1 M of Na ₂ SO ₃ electrolyte	118
5.31	Photoconversion efficiency as a function of applied voltage versus (Ag/AgCl) of: Bi ₂ S ₃ /ZnO NRAs prepared at different annealing temperatures: (a) as-deposited; (b) 100 °C; (c) 200 °C; (d) 300 °C; (e) 400 °C; (f) 500 °C at illumination intensity of 100 mWcm ⁻² in 0.1M Na ₂ SO ₃ and 0.1M Na ₂ S electrolyte mixture	119
5.32	Schematic band alignment of the heterostructured Bi ₂ S ₃ /ZnO NRAs /ITO binary nanostructure	120
6.1	FE-SEM images at two different magnification ($\times 25,000$ and $\times 50,000$) of (a) ZnO NRAs, Ag ₂ S/ZnO NRAs prepared at different SILAR cycles: (b) 4 cycles; (c) 6 cycles; (d) 8 cycles; (e) 12 cycles	123
6.2	Photographic image of Ag ₂ S/ZnO NRAs samples at different SILAR cycle numbers: (a) 4cycles; (b) 6 cycles; (c) 8 cycles; (d) 10 cycles; (e) 12 cycles	124

6.3	X-ray diffractogram of: (a) bare ZnO NRAs; Ag ₂ S/ZnO NRAs/ITO prepared at different SILAR cycles: (b) 4 cycles; (c) 6 cycles; (d) 8 cycles; (e) 10 cycles and (f) 12 cycles	125
6.4	(A) UV-Vis Spectra; (B) the optical bandgap energy curves of: (a) ZnO NRAs/ITO; Ag ₂ S/ZnO NRAs/ITO prepared at different SILAR cycles: (b) 4 cycles; (c) 6 cycles; (d) 8 cycles; (e) 10 cycles and (f) 12 cycles	126
6.5	Linear sweep voltammograms obtained at the scan rate of 20 mV s ⁻¹ at applied potentials from -0.5 V to +1.0 V under illumination intensity of 100 mWcm ⁻² in 0.1M Na ₂ S and Na ₂ SO ₃ electrolyte for: (a) bare ZnO NRAs/ITO; Ag ₂ S/ZnO NRAs/ITO prepared at different SILAR cycles: (b) 4 cycles; (c) 6 cycles; (d) 8 cycles; (e) 10 cycles and (f) 12 cycles	127
6.6	Photoconversion efficiency values as a function of applied voltage vs. Ag/AgCl of Ag ₂ S/ ZnO NRAs at different SILAR cycles: (a) 4 cycles; (b) 6 cycles; (c) 8 cycles; (d) 10 cycles; (f) 12 cycles under illumination intensity (100 mW cm ⁻²) in mixture of 0.1 M Na ₂ S and Na ₂ SO ₃	128
6.7	FE-SEM images at two different magnification (\times 25,000 and \times 50,000) of (a) ZnO NRAs, Ag ₂ S/ZnO NRAs prepared at different dipping time: (b) 20 s; (c) 60 s; (d) 80 s;(e) 100 s	130
6.8	XRD patterns of: (a) ZnO nanorods decorated with Ag ₂ S nanoparticles with different dipping time: (b) 20 s; (b) 40 s; (c) 60 s; (d) 80 s; (f) 100 s	131
6.9	(A) UV-Vis Spectra; (B) bandgap energy curves of (a) ZnO NRAs/ ITO and Ag ₂ S/ZnO NRAs/ITO prepared at different dipping time : (b) 20 s; (b) 40 s; (c) 60 s; (d) 80 s; (f) 100 s The inset of Figure A shows the E _g changes at different dipping time	132
6.10	Linear sweep voltammograms obtained at the scan rate of 20 mVs ⁻¹ at applied potentials from -0.5V to +1.0 V under illumination intensity of 100 mWcm ⁻² in 0.1 M Na ₂ S and Na ₂ SO ₃ electrolyte for: (a) ZnO NRAs/ITO; Ag ₂ S/ZnO NRAs/ITO at different dipping time : (b) 20 s; (c) 40 s; (d) 60 s; (e) 80 s; (f) 100 s	133
6.11	XRD patterns of (a) ZnO nanorods decorated with Ag ₂ S nanoparticles at different cationic concentration: (b) 0.01 M; (c) 0.02 M; (d) 0.04 M; (e) 0.06M; (f) 0.08 M	135
6.12	FE-SEM images of (a) bare ZnO NRAs; and ZnO nanorods decorated with Ag ₂ S nanoparticles , (b) 0.01 M; (c) 0.02 M; (d) 0.06 M; (e) 0.08 M at different magnifications (\times 25,000 and \times 50,000)	136

6.13	(A) UV-Vis Spectra; (B) bandgap energy curves of: (a) ZnO NRAs/ITO and Ag ₂ S/ZnO NRAs/ITO prepared at different cationic concentration: (b) 0.01 M; (c) 0.02 M; (d) 0.04 M; (e) 0.06 M; (f) 0.08 M. Eg values at different cationic concentration is shown in the insets of figure	137
6.14	Linear sweep voltammograms obtained at the scan rate of 20 mV s ⁻¹ at applied potentials from -0.5 V to +1.0 V under illumination intensity of 100 mWcm ⁻² in 0.1M Na ₂ S and Na ₂ SO ₃ electrolyte for: (a) ZnO NRAs/ITO; Ag ₂ S/ZnO NRAs/ITO at various cationic concentration: (b) 0.01 M; (c) 0.02 M; (d) 0.04 M; (e) 0.06 M;(f) 0.08 M	138
6.15	XRD patterns of (a) : pure ZnO NRAs and Ag ₂ S/ZnO NRAs at different cationic pH;(b) 3; (c) 4; (d) 5; (e) 6; (f) 7	139
6.16	FE-SEM images of bare ZnO NRAs (a), and ZnO nanorods decorated with Ag ₂ S nanoparticles at different pH: (b) 3; (c) 4; (d) 5; (e) 6; (f) 7 at (\times 25,000 and \times 50,000) magnification	140
6.17	(A) UV-Vis spectra; (B) bandgap energy curves of: (a) ZnO NRAs/ITO and Ag ₂ S/ZnO NRAs/ITO prepared at different cationic pH: (b) 3; (c) 4; (d) 5; (e) 6; (f) 7. Eg values at different cationic pH is shown in the insets of figure	141
6.18	Linear sweep voltammograms obtained at the scan rate of 20 mVs ⁻¹ at applied potentials from -0.5 V to +1.0 V under illumination intensity of 100 mWcm ⁻² in 0.1M Na ₂ S and Na ₂ SO ₃ electrolyte for: (a) ZnO NRAs/ITO; Ag ₂ S/ZnO NRAs/ITO at various cationic pH: (b) 3; (c) 4; (d) 5; (e) 6; (f) 7	142
6.19	Photoconversion efficiency values as a function of applied voltage vs. Ag/AgCl of Ag ₂ S/ZnO NRAs at different AgNO ₃ pH: (a) 3; (b) 4; (c) 5; (d) 6; (e) 7 under illumination intensity (100 mW cm ⁻²) in mixture of 0.1 M Na ₂ S and of Na ₂ SO ₃	143
6.20	XRD patterns of (a) : pure ZnO NRAs and Ag ₂ S/ZnO NRAs at different annealing temperatures: (b) as-deposited; (c) 100 °C; (d) 200 °C;(e) 300 °C; (f) 400 °C and (g) 500 °C for 1 h with heating rate of 2 degree/ min in N ₂ atmosphere	144
6.21	The EDS spectra of Ag ₂ S/ZnO NRAs annealed at 400°C for 1 h with heating rate of 2 degree/min in N ₂ atmosphere	145
6.22	High resolution XPS spectrum of Ag ₂ S/ZnO NRAs/ITO-400 °C for 1 h with heating rate of 2 degree/min in N ₂ atmosphere - survey spectrum	146
6.23	XPS spectra of Zn-2p (a); (b) O-1s; (c) Ag-3d; (d) S-2p elements in Ag ₂ S/ZnO/ITO annealed at 400 °C	147

6.24	Raman spectra of the optimum sample Ag ₂ S/ZnO NRAs/ITO annealed at 400 °C for 1 h with heating rate of 2 degree/min in N ₂ atmosphere	148
6.25	FE-SEM images of (a) bare ZnO NRAs, ZnO NRAs decorated with Ag ₂ S nanoparticles annealed at different temperatures (b) as-deposited ; (c) 100 °C; (d) 200 °C; (e) 400 °C; (f) 500°C. Higher magnification is shown in the inset of figure	149
6.26	(a) TEM images and (b) HRTEM images of the optimal sample of Ag ₂ S/ZnO NRAs annealed at 400 °C for 1 h with heating rate of 2 degree/min in N ₂ atmosphere	150
6.27	(A) UV-Vis Spectra; (B) the optical bandgap energy curves of: (a) ZnO NRAs/ITO; (b) Ag ₂ S/ZnO NRAs/ITO as-deposited and Ag ₂ S/ ZnO NRAs/ITO annealed at (c) 100 °C;(d) 200 °C ; (e) 300 °C; (f) 400 °C; (g) 500 °C. Eg values at different annealing temperatures is shown in the inset of figure	151
6.28	Linear sweep voltammograms of (a) bare ZnO NR; (b) as -deposited Ag ₂ S/ZnO NRAs/ITO, and Ag ₂ S/ZnO NRAs/ITO annealed at (c) 100 °C; (d)200 °C; (e) 300 °C; (f) 400 °C; (g) 500 °C for 1 h, obtained at the scan rate of 20 mV s ⁻¹ at the applied potential from -0.5 V to + 1.0 V under illumination intensity (100 mW/ cm ²) in 0.1 M Na ₂ S and 0.1 M Na ₂ SO ₃ electrolyte	152
6.29	Photoconversion efficiency values as a function of applied voltage vs. Ag/AgCl of Ag ₂ S/ZnO NRAs/ITO at different annealing temperatures: (a) as -deposited; (b) 100 °C; (b) 200 °C; (c) 300 °C; (d) 400 °C; (f) 500 °C for 1 h, under illumination intensity (100 mW/cm ²) in 0.1 M Na ₂ S and 0.1 M Na ₂ SO ₃	153
6.30	Schematic band alignment of Ag ₂ S/ZnO NRAs binary heterostructure photoanode	154
7.1	XRD patterns of (a): pure ZnO NRAs and Bi ₂ S ₃ /Ag ₂ S/ZnO NRAs /ITO at different SILAR cycles : (b) 1 cycle; (c) 3 cycles; (d) 5 cycles; (e) 7 cycles; (f) 9 cycles	157
7.2	(A) UV-Vis spectra; (B) the optical bandgap energy curves of: (a) ZnO NRAs/ITO; (b) Bi ₂ S ₃ /Ag ₂ S/ZnO NRAs/ITO prepared at different SILAR cycles : (b) 1 cycle; (c) 3 cycles; (d) 5 cycles;(e) 7 cycles; (f) 9 cycles. Eg values at different SILAR cycles is shown in the inset of figure	158
7.3	Linear sweep voltammograms of (a) bare ZnO NR; (b) as -deposited Ag ₂ S/ZnO NRAs/ITO; (c) Ag ₂ S/ZnO NRAs/ITO annealed 400 °C; and Bi ₂ S ₃ /Ag ₂ S/ZnO NRAs/ITO prepared at different SILAR cycles at (d) 1 cycle; (e) 3 cycles; (f) 5 cycles;(g) 7 cycles; (h) 9 cycles. obtained at the scan rate of 20 mV s ⁻¹ at the applied potential from -	

	0.5 V to + 1.0 V under illumination intensity (100 mW/ cm ²) in 0.1 M Na ₂ S and 0.1 M Na ₂ SO ₃ electrolyte	159
7.4	Photoconversion efficiency values as a function of applied voltage vs. Ag/AgCl of: (a) ZnO NRAs; (b) Ag ₂ S/ZnO NRAs/ITO-400 °C; Bi ₂ S ₃ /Ag ₂ S/ZnO NRAs/ITO prepared at different SILAR cycles at (c) 1 cycle; (d) 3 cycles; (e) 5 cycles;(f) 7 cycles; (g) 9 cycles under illumination intensity (100 mW/cm ²) in 0.1 M Na ₂ S and 0.1 M Na ₂ SO ₃	160
7.5	FE-SEM images of: (a) Ag ₂ S/ZnO NRAs-400 °C, Bi ₂ S ₃ /Ag ₂ S/ZnO NRAs/ITO prepared at different SILAR cycles at (b) 1 cycle; (c) 3 cycles; (d) 5 cycles;(e) 7 cycles; (f) 9 cycles. Higher magnification (\times 50,000) of the images is in the insets of figures	161
7.6	XRD patterns of (a): pure ZnO NRAs and Bi ₂ S ₃ /Ag ₂ S/ZnO NRAs/ITO at different dipping time: (b) 5 s; (c) 10 s; (d) 15 s;(e) 20 s; (f) 25 s	162
7.7	(A) UV-Vis Spectra; (B) the optical bandgap energy curves of: (a) ZnO NRAs/ITO; (b) Bi ₂ S ₃ /Ag ₂ S/ZnO NRAs/ITO prepared at different dipping time: (b) 5 s; (c) 10 s; (d) 15 s;(e) 20 s; (f) 25 s. Eg values at different dipping time is shown in the inset of figure	163
7.8	Linear sweep voltammograms of (a) bare ZnO NR; (b) as -deposited Ag ₂ S/ZnO NRAs/ITO; (c) Ag ₂ S/ZnO NRAs/ITO annealed 400 °C; and Bi ₂ S ₃ /Ag ₂ S/ZnO NRAs/ITO prepared at different dipping time: (d) 5 s; (e) 10 s; (f) 15 s;(g) 20 s; (h) 25 s obtained at the scan rate of 20 m V s ⁻¹ at the applied potential from -0.5 V to +1.0 V under illumination intensity (100 mW/ cm ²) in mixture of 0.1 M Na ₂ S and M Na ₂ SO ₃ electrolyte	164
7.9	Photoconversion efficiency values as a function of applied voltage vs. Ag/AgCl of (a) bare ZnO NRAs; (b) Ag ₂ S/ZnO NRAs-400 °C; Bi ₂ S ₃ /Ag ₂ S/ZnO NRAs/ITO prepared at different dipping time: (c) 5 s; (d) 10 s; (e) 15 s;(f) 20 s; (g) 25 s under illumination intensity (100 mW/cm ²) in 0.1 M Na ₂ S and 0.1 M Na ₂ SO ₃	165
7.10	FE-SEM images of (a) Ag ₂ S/ZnO NRAs/ITO annealed 400 °C; and Bi ₂ S ₃ /Ag ₂ S/ZnO NRAs/ITO prepared at different dipping time: (b) 5 s; (c) 10 s; (d) 15 s;(e) 20 s; (f) 25 s. \times 50,000 magnification of the images is in the insets of figures	166
7.11	FE-SEM images of (a): bare ZnO NRAs and Bi ₂ S ₃ /Ag ₂ S/ZnO NRAs /ITO electrode synthesised at different annealing temperatures: (b) as-deposited; (c) 100 °C; (d) 200 °C; (e) 400 °C; (f) 500 °C for 1h with heating rate of 2degree/min in N ₂ atmosphere. Magnification (\times 50,000 is shown in the insets of figures	168

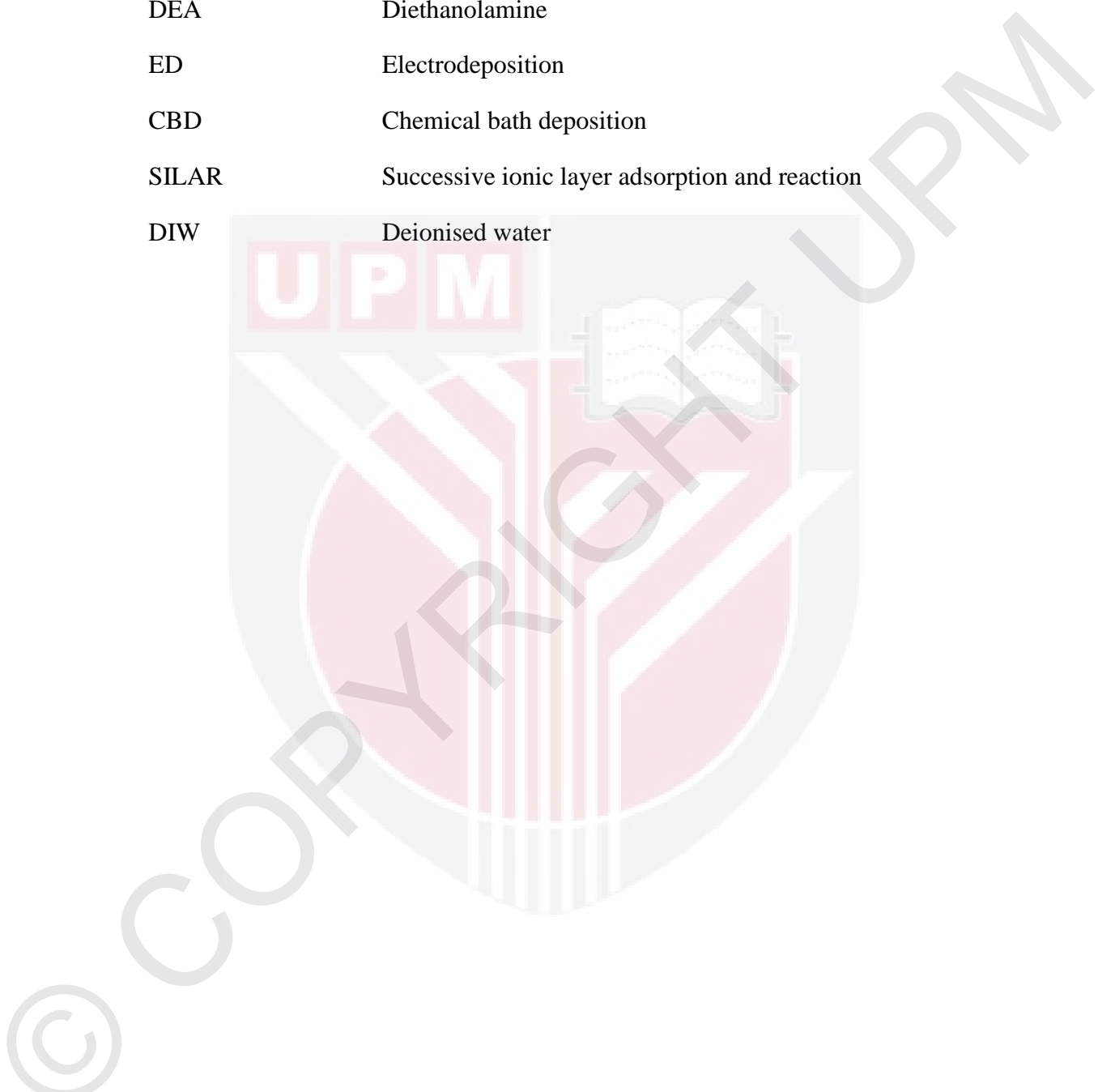
7.12	EDS pattern and elemental mapping (EELS) of Bi ₂ S ₃ /Ag ₂ S/ZnO NRAs /ITO annealed at 400 °C 1h with heating rate of 2 degree/min in N ₂ atmosphere	169
7.13	(a) TEM and (b) HR-TEM image of the optimum sample Bi ₂ S ₃ /Ag ₂ S /ZnO NRAs/ITO annealed at 400 °C for 1 h in N ₂ atmosphere	170
7.14	XPS spectra of Bi ₂ S ₃ /Ag ₂ S/ZnO NRAs/ITO heterostructure (optimal sample annealed at 400 °C): (a) the XPS survey spectra of Bi ₂ S ₃ /Ag ₂ S/ZnO/ITO; (b) Zn 2p spectra ; (c) O 1s spectra; (d) Bi 4f and S 2p spectra; (e) Ag 3d spectra	171
7.15	XRD diffractogram of : (a) ZnO NRAs/ITO; Bi ₂ S ₃ /Ag ₂ S/ZnO NRAs /ITO prepared at different annealing temperatures : (b) as-deposited; (c) 100 °C; (d) 200 °C; (e) 300 °C; (f) 400 °C; (g) 500 °C	172
7.16	(A) UV-Vis spectra; (B) bandgap energy curves of: (a) ZnO NRAs/ ITO; (b) Bi ₂ S ₃ /Ag ₂ S/ZnO NRAs/ITO-as deposited; (c) 100 °C; (d) 200 °C;(e) 300 °C; (f) 400 °C; (g) 500 °C for 1 h in N ₂ air. The changes in optical band gap energy values at different annealing temperatures is shown in the inset of figure	173
7.17	Linear sweep voltammograms obtained at the scan rate of 20 mVs ⁻¹ at applied potentials range from -0.5 V to +1.0 V under illumination intensity of 100 mWcm ⁻² in 0.1M Na ₂ S and Na ₂ SO ₃ electrolyte for: (a) ZnO NRAs and Bi ₂ S ₃ /Ag ₂ S/ZnO NRAs/ITO at different annealing temperatures :(b) as-deposited; (c) 100 °C; (d) 200 °C;(e) 300 °C; (f) 400 °C; (g) 500 °C for 1 h in N ₂ air	174
7.18	Photoconversion efficiency as a function of applied voltage versus (Ag/AgCl) of: (a) bare ZnO NRAs/ITO; Bi ₂ S ₃ (7)/Ag ₂ S (6)/ZnO NRAs/ITO at different annealing temperatures :(b) as-deposited; (c) 100 °C; (d) 200 °C; (e) 300 °C; (f) 400 °C; (g) 500 °C for 1 h in N ₂ air under illumination intensity of 100 mWcm ⁻² in 0.1M Na ₂ SO ₃ and 0.1M Na ₂ S electrolyte mixture	175
7.19	Schematic of the relative energy levels and ideal cascade band structure in Bi ₂ S ₃ /Ag ₂ S /ZnO NRAs/ITO heterostructure ternary system	176
7.20	X-ray diffractogram of: (a) bare ZnO NRAs; (b) Bi ₂ S ₃ /ZnO NRAs/ ITO; (c) Ag ₂ S/ZnO NRAs; (d) Bi ₂ S ₃ /Ag ₂ S /ZnO NRAs/ITO	177
7.21	Plane view FE-SEM images with cross-sectional of: (a-b) bare ZnO NRAs; (c-d) Bi ₂ S ₃ /ZnO NRAs/ITO; (e-f) Ag ₂ S/ZnO NRAs/ITO; (g-h) Bi ₂ S ₃ /Ag ₂ S /ZnO NRAs/ITO	178
7.22	TEM images of : (a) bare ZnO NRAs; (b) Bi ₂ S ₃ /ZnO NRAs/ITO; (c) Ag ₂ S/ZnO NRAs/ITO; (d) Bi ₂ S ₃ /Ag ₂ S /ZnO NRAs/ITO	179

7.23	HRTEM image of : (a) Bi ₂ S ₃ /ZnO NRAs/ITO; (b) Ag ₂ S/ZnO NRAs /ITO; (c) Bi ₂ S ₃ /Ag ₂ S /ZnO NRAs/ITO	180
7.24	EDS patterns of: (a) Bi ₂ S ₃ /ZnO NRAs/ITO; (b) Ag ₂ S/ZnO NRAs /ITO; (c) Bi ₂ S ₃ /Ag ₂ S /ZnO NRAs/ITO	181
7.25	UV-Vis spectra of : (a) bare ZnO NRAs/ITO; (b) Bi ₂ S ₃ /ZnO NRAs /ITO; (c) Ag ₂ S/ZnO NRAs/ITO; (d) Bi ₂ S ₃ /Ag ₂ S /ZnO NRAs/ITO	183
7.26	Optical bandgap energy curves of: (a) bare ZnO NRAs/ITO; (b) Bi ₂ S ₃ /ZnO NRAs/ITO; (c) Ag ₂ S/ZnO NRAs/ITO; (d) Bi ₂ S ₃ /Ag ₂ S /ZnO NRAs/ITO	183
7.27	Linear sweep voltammograms of : (a) bare ZnO NRAs/ITO; (b) Bi ₂ S ₃ /ZnO NRAs/ITO; (c) Ag ₂ S/ZnO NRAs/ITO; (d) Bi ₂ S ₃ /Ag ₂ S /ZnO NRAs/ITO under illumination intensity of 100 mWcm ⁻² in 0.1M Na ₂ SO ₃ and 0.1M Na ₂ S electrolyte mixture	185
7.28	Photoconversion efficiency values as a function of applied voltage versus Ag/AgCl of : (a) bare ZnO NRAs/ITO; (b) Bi ₂ S ₃ /ZnO NRAs /ITO; (c) Ag ₂ S/ZnO NRAs/ITO; (d) Bi ₂ S ₃ /Ag ₂ S /ZnO NRAs/ITO under illumination intensity (100 mW cm ⁻²) in 0.1 M Na ₂ S and 0.1 M Na ₂ SO ₃ electrolyte	186
7.29	Plot of photoconversion efficiency values versus of : bare ZnO NRAs /ITO; Bi ₂ S ₃ /ZnO NRAs/ITO; Ag ₂ S/ZnO NRAs/ITO; Bi ₂ S ₃ /Ag ₂ S /ZnO NRAs/ITO	187

LIST OF ABBREVIATIONS

NRs	Nanorods
NRAs	Nanorods Arrays
NPs	Nanoparticles
PEC	Photoelectrochemical
UV-Vis	Ultraviolet-visible spectroscopy
EDS	Energy Dispersive X-Ray Spectroscopy
XRD	X-ray diffraction
FE-SEM	Field Emission Scanning Electron Microscopy
XPS	X-ray photoelectron spectroscopy
TEM	Transmission Electron Microscopy
HR-TEM	High Resolution-Transmission Electron Microscopy
SAED	Selected Area Electron Diffraction
EELS	Electron Energy Loss Spectrometer
ITO	Indium Tin Oxide
E_g	Optical bandgap energy
C.B.	Conduction band
V.B.	Valence band
e	Electron
h	Hole
J_{ph}	Photocurrent density
V_{app}	Voltage applied
LSV	Linear Sweep Voltammetry
<i>Red.</i>	Redaction
<i>Ox.</i>	Oxidation
WE	Working electrode

CE	Counter electrode
RE	Reference electrode
HMTA	Hexamethylenetetramine
DEA	Diethanolamine
ED	Electrodeposition
CBD	Chemical bath deposition
SILAR	Successive ionic layer adsorption and reaction
DIW	Deionised water



CHAPTER 1

INTRODUCTION

1.1 Background of the Study

The main urgent energy issue is to concentrate on identifying the resources in the generation and supply of energy that can substitute fossil fuels to meet the world's tremendous energy consumption. Renewable energy resources such as geothermal and tidal power and other renewable energy resources possibilities like wind power, biofuels, hydropower, and solar energy should be considered as potential replacements by the turn of the century. Since the amount of energy usage almost parallels the rate of economic growth and private satisfaction, it is clear that humanity's survival at the current developmental rate will depend on appropriate and adequate energy accessibility. Current circumstances call for contamination-free and less costly sources of energy that can be sourced by harnessing solar energy (Islam et al., 2020) to avoid more crisis in the environment. The most attractive possibility is solar-based energy because it is available in abundance to the extent of ten thousand times the total annual energy use. Furthermore, it will also neither affect the equalisation of our planet's heat energy nor will it cause any contamination.

Several technologies have efficiently utilised the spectrum of visible light, namely photovoltaic (Mishra & Tiwari, 2020), photochemical, photoelectrochemical, and the photothermal cells (Manassen et al., 1976). A number of review articles (Ahmed & Dincer, 2019; Rattanawarinchai et al., 2018; Kumar et al., 2017) have been published in the field of photoelectrochemical conversion. For two to three decades, many attempts have been made with separate solar conversion systems. As a result of the emergence of the field of photoelectrochemistry, the connection between photovoltaic devices and electrochemical devices was established and consequential developments such as photoelectrochemical solar cells (PECs) were used to further strengthen the field (Li et al., 2013).

Among the above methods, photoelectrochemical cells have lately achieved popularity as an inexpensive technique to convert solar energy into chemical then electrical energy to achieve high conversion efficiency. Furthermore, one of the interesting study elements in this sector is the search for cost-effective materials for the photoelectrodes. Therefore, several attempts were made to increase the quality performance of the photoanode materials.

Currently, the study of semiconductor nanomaterials has been reinforced as a photoanode in photoelectrochemical cells and is growing rapidly. In addition, owing to their outstanding structural flexibility along with other appealing characteristics, metal oxide semiconductor nanomaterials have gained more attention. The metal oxide nanostructures achieve appealing characteristics due to their bulk, such as chemical sensing, photoelectrochemical efficiency, and photodetection, as well as

characteristics associated with their highly anisotropic geometry and size confinement (Lu et al., 2006). The composites of novel and traditional characteristics with distinctive nanostructure impacts make the investigation of novel metal oxide nanostructures a quiet remarkable topic in research and development from both an essential and a wide-ranging viewpoint. Due to its distinctive features, simple crystallisation at low temperature, elevated electron mobility, its wide optoelectronic applications, Zinc oxide (ZnO) has received significant recognition among distinct metal oxides. In particular, ZnO nanostructures (NSs) are deeply focused as they can be synthesised with distinct morphologies through various methods (Xu & Wang, 2011). Several decades of research have resulted in numerous methods of synthesising ZnO nanostructure as well as sensitizing ZnO. One of the most prevalent methods is the successive ionic layer adsorption and reaction (SILAR) method, hydrothermal (HT) technique and sol-gel spin coating (Holi et al., 2019; Nikam et al., 2015; Saleem et al., 2012).

The one-dimensional ZnO nanorods (NRAs) structure has been extensively studied, particularly among diversified nanostructures, as it offers a wide surface area. A large surface area is the main factor in achieving high effectiveness in PEC applications (Desai et al., 2020). ZnO properties such as, wide bandgap energy (3.37 eV), 60 meV strong exciton energy, $300 \text{ cm}^2 \text{ v}^{-1} \cdot \text{s}^{-1}$ high electronic mobility that drawn the attention of the research community extend back to 1935, specifically in the application sector for low wavelength optoelectronics energy. Despite its many strengths over ZnO nanorods as a broad direct bandgap semiconductor, however ZnO's applications in optoelectronics are limited by the unavailability of visible light harvesting (Xu et al., 2020). ZnO nanorods should, therefore, be altered to enhance the absorption harvest in the visible light spectrum. This can be accomplished by sensitising the surface to adjust the comparatively large bandgap. Great efforts have been made through different methods, such as organic dye doping (Norton et al., 2004), synthesising heterostructure (Kumar et al., 2017), dye sensitisation (Kilic, 2019) and sensitisation by using narrow bandgap energy chalcogenide materials (Khot et al., 2015). Due to their strong absorption coefficient, high stability, flexible bandgap and great matching bandgap with visible range, narrow bandgap energy metal chalcogenide semiconductors have been selected among the afore-mentioned approaches (Zhao et al., 2019).

Since their implementation in optoelectronic systems, narrow bandgap metal chalcogenide are promising candidates for sensitising ZnO nanorods. Narrow bandgap energy metal chalcogenide semiconductors such as bismuth sulphide (Bi_2S_3) and silver sulphide (Ag_2S) could be appropriate photosensitisers for ZnO NRAs to manufacture photo-electrodes that can use both the characteristics of wide and narrow bandgap energy materials and enhance the hosting material's light-harvesting capability. Due to its narrow optical bandgap inset $1.3 \sim 1.7 \text{ eV}$ and a wide range of electronic device applications, Bi_2S_3 was adopted as a reliable photosensitizer (Arumugam et al., 2018). Ag_2S is also appropriate for qualifying as a non-toxic, narrow bandgap energy of $0.9 \sim 1.05 \text{ eV}$ which makes it an efficient photovoltaic semiconductor material (Holi et al., 2018). As a result, composite materials (i.e. small bandgap bases / metal oxide) based semiconductor nanofilms have become essential

for enhancing the effectiveness of photoconversion due to their high conversion, electrolyte system stability, low-cost production, and flexibility. Due to their affordable synthesis and low used amount of starting materials, thin films nanomaterials are favoured, which implies large-scale manufacturing. It should be noted that the properties of photoelectrochemical cells (PECs) for nanocomposite materials can be significantly improved by (i) controlling the ZnO NRAs preparation condition to improve the aspect ratio to accommodate the photosensitiser; (ii) ZnO sensitisation with narrow band gap materials such as Bi_2S_3 and Ag_2S to increase its ability to absorb more visible light.

1.2 Problem Statement

ZnO is the most promising contender because of its high earth plenty, nontoxicity as well as exceptional physical and chemical features for diverse photovoltaic uses. Many of these applications have used thin film ZnO nanostructure which is considered an ideal alternative to the high costly single crystal, silicon-based photoelectrochemical cells. ZnO is a typical II–VI semiconductor compound with a hexagonal phase of wurtzite, which has excellent electronic and optical properties. This is expressed in its properties such as 3.37 eV wide bandgap energy and substantial 60 meV excitonic binding energy at room temperature compared to other materials with a wide bandgap energy such as TiO_2 . However, ZnO's wide bandgap energy absorbs only a small portion of visible spectrum of light. Sensitising the surface of ZnO nanorods can increase the visible light harvesting. Sensitising the ZnO NRAs surface can be achieved with doping organic dyes, using nanocomposite materials, or doping with narrow bandgap materials. Since several sensitises involving organic dyes have been widely studied, inorganic metal chalcogenide with narrow bandgap energy values have gained significant attention among researchers owing to their excellent absorption over a wide wavelength range, great stability, adjustable bandgap, and high conversion efficiency. Numerous studies have indicated sensitization of ZnO nanorods employing inorganic chalcogenide semiconducting nanoparticles like CdS (Nikam et al., 2016), PbS (Li Xianchang et al., 2016), Ag_2S (Holi et al., 2018), Cu_2O (Messaoudi et al., 2015), CdSe (Nikam et al., 2018), and Bi_2S_3 (Velanganni et al., 2018) by employing various approaches which shows a range of possible uses and a remarkable enhancement in their outcomes compared to the intrinsic structure.

Among the metal chalcogenide narrow band materials described above, such as bismuth sulphide (Bi_2S_3) and silver sulphide (Ag_2S) can then be used efficiently to improve the photo response of ZnO NRAs. It is well known that both Bi_2S_3 and Ag_2S have suitable E_{gS} within the visible light spectrum and can be regarded as proper materials for enhancing the ZnO light harvesting. Therefore, their narrow bandgap energy may efficiently expand the ZnO absorption range from the UV region to the visible light spectrum region. Additionally, the two narrow band metal chalcogenides have been used to co-sensitise ZnO to enhance the alignment of the bandgaps reflecting significant improvement in optical and electrical properties. However, one of the most essential problems that can be faced when using sensitiser materials with narrow band gap energy, is the high rate of electron-hole pairs recombination caused by a strong exciton binding energy.

The literature review indicates that the performance of binary photoanodes of $\text{Bi}_2\text{S}_3/\text{ZnO}$ and $\text{Ag}_2\text{S}/\text{ZnO}$ fabricated by SILAR method needs more investigations to improve the ability of the photoconversion efficiency of PEC. Moreover, there is no report so far on deposition of the ternary construction of $\text{Bi}_2\text{S}_3/\text{Ag}_2\text{S}/\text{ZnO}$ for photoelectrochemical applications. Hydrothermal approach and successive ionic layer adsorption and reaction (SILAR) method have been used for synthesis of ZnO NRAs and nanocomposite samples, respectively. The two methods are simple, inexpensive, low preparation temperature, controllable preparation parameters and eco-friendly, all of which encourage large industrial production. This study introduces an essential contribution for improving bandgap structure using binary, ternary nanocomposite for PECs application via simplified methods.

1.3 Study Objectives

In a world where natural resources are not abundant and our dependence on them continues to grow, great interest has always been shown in finding new technology that can support our demands without the consumption of non-renewable resources. One of the most promising areas is photovoltaic devices-photoelectrochemical cells. Semiconductor nanomaterials have drawn much attention as a promising candidate for the research and development of the highly converted photoelectrochemical cell. Nanocomposite semiconductors such as $\text{Bi}_2\text{S}_3/\text{ZnO}$, $\text{Ag}_2\text{S}/\text{ZnO}$ and $\text{Bi}_2\text{S}_3/\text{Ag}_2\text{S}/\text{ZnO}$ have traditionally demonstrated significant flexibility in their fundamental features. Bi_2S_3 and Ag_2S nanomaterials have been extensively discussed due to their distinctive photoelectronic, photochemical and photocatalytic properties that are totally different from their bulk counterparts, their characteristics are critically dependent on the particle shape, size, and surface composition.

This research involves fundamental research on synthesis of nanostructure, surface modification and application of nano thin film semiconductors for clean and environmentally-friendly energy conversion.

This project aims to use two convenient low-cost techniques to synthesise binary heterostructured $\text{Bi}_2\text{S}_3/\text{ZnO}/\text{ITO}$, $\text{Ag}_2\text{S}/\text{ZnO}/\text{ITO}$, and ternary $\text{Bi}_2\text{S}_3/\text{Ag}_2\text{S}/\text{ZnO}/\text{ITO}$ photoanode for photoelectrochemical applications. Simple and low-cost hydrothermal method has been used for fabricating ZnO NRAs while SILAR method has been used to deposit narrow band gap energy-based metal chalcogenides on ZnO NRAs. Moreover, increasing the aspect ratio of ZnO NRAs by adjusting the distribution of nucleation sites and controlling the temperature, the growth period is one of the imperative keys for high conversion efficiency. In addition, the morphological, compositional structure, optical features and photoelectrochemical performance of the electrodes have been researched carefully.

The clearly defined objectives of this research are:

1. To improve the surface area of the ZnO nanostructure layers via controlling the annealing temperature of ZnO NPs seed layer, controlling growth temperature and growth time of ZnO NRAs by using sol-gel spin coating technique and hydrothermal method, respectively.
2. To enhance ZnO nanostructure's structural, optical and photoelectrochemical characteristics by depositing Bi₂S₃ and Ag₂S as binary nanocomposite heterostructure into ZnO using the SILAR technique and to characterise the optical, morphological and photoelectrochemical performance of binary photoanodes
3. To fabricate and characterise Bi₂S₃ and Ag₂S as co-sensitised ZnO nanorods to improve the alignment of bandgaps to achieve improved optical characteristics and photoelectrochemical efficiency.
4. To evaluate the photoconversion efficiencies of photoelectrochemical cells with different fabricated photoanodes ZnO NPs/ITO, ZnO NRAs/ITO, binary heterostructured Bi₂S₃/ZnO/ITO, Ag₂S/ZnO/ITO, and ternary heterostructured Bi₂S₃/Ag₂S/ZnO/ITO.

1.4 Significance of the Study

Global warming and climate change are aspects of great concern as we move further forward into the 21st century. As world energy consumption increases and fossil fuel reserves decline, clean and renewable energy sources have never been more demanded. Studies on renewable energy sources, which are plentiful, environmentally sustainable, renewable, and cost-effective, increased dramatically due to rising energy demand and limitations on existing energy sources such as coal, oil, and natural gas. Solar energy clearly shows the greatest promise represented by the three most prevalent sources of renewable energy. The sun radiates have sufficient energy over an hour to power the Earth for one year. A world map with horizontal solar irradiation globally shows that sunlight can power almost every country to meet their individual energy needs. The rapid increase in research of solar energy has generated some prominent trends in recent years. Effectiveness of the commercial panel has risen, while expenditure has decreased proportionately. Due to their streamlined production and high photoconversion efficiency, photoelectrochemical cells based on photosensitised narrow-band materials are considered one of the most important options for using abundant solar energy. This research would yield an important contribution to the ongoing search for ZnO nanostructure sensitizers in order to improve light harvesting for photoelectrochemical applications.

1.5 Scope of the Study

In this study, two different hierarchical hybrid materials are developed by simple successive ionic layer adsorption and reaction (SILAR) method and their morphological structures, optical and electrical properties effects on the

photoelectrochemical cells performance are investigated extensively. Zinc oxide is used as a template for the growth of binary and ternary hierarchical nanostructures on ITO substrates. In all instances, the acquired heterostructure binary photoanode is fabricated through three basic steps: (i) preparation of high density ZnO nanoparticles seed layer via sol-gel spin coating; (ii) synthesising optimised well-aligned ZnO nanorod arrays using simplified hydrothermal method; (iii) photosensitising ZnO NRAs using narrow bandgap energy metal chalcogenides with SILAR technique. The motivation of this research is the investigating the effect of Bi_2S_3 and Ag_2S modifying the surface of ZnO NRAs on their performance as a photoanode in photoelectrochemical cells. Control of the production condition of $\text{Bi}_2\text{S}_3/\text{ZnO}$ NRAs/ITO, $\text{Ag}_2\text{S}/\text{ZnO}$ NRAs/ITO arrays such as SILAR cycle number, dipping time, cationic concentration, pH, and annealing temperature is essential to enhance the ability of photosensitised-ZnO NRAs to harvest visible light. This thesis is divided into eight chapters: Chapter one includes the research background, problem statement, and study objectives, followed by study significance, and then study scope, which concludes the chapter. Chapter two highlights the working principles of semiconductor electrodes in photoelectrochemical cells and related literature on methods of thin film synthesis heterostructure and characterization techniques. Chapter three outlines the methods and processes used in this study. All the fabrication procedures for ZnO NPs/ITO seed layer, ZnO NRAs/ITO arrays, binary heterostructure ($\text{Bi}_2\text{S}_3/\text{ZnO}/\text{ITO}$, $\text{Ag}_2\text{S}/\text{ZnO}/\text{ITO}$, and ternary structure) and several preparations adjusting variables are described and explained. Chapter four includes the data analysis and discussion of the findings and the outcomes of the experiments related to ZnO nanoparticles seed layers and ZnO NRAs. Chapter five and six include the data analysis and findings discussion of binary heterostructured photoanode which are $\text{Bi}_2\text{S}_3/\text{ZnO}$ NRAs and $\text{Ag}_2\text{S}/\text{ZnO}$ NRAs/ITO, respectively. While chapter seven includes the data analysis and discussion of results of the ternary heterostructure $\text{Bi}_2\text{S}_3/\text{Ag}_2\text{S}/\text{ZnO}$ NRAs/ITO. The comparison between the plain ZnO NRAs, binary and ternary nanocomposite photoanode has been presented in chapter seven too. Chapter eight presents the conclusions drawn from the research and finally makes recommendations for further related research.

REFERENCES

- Abderrahmane, B., Djamilia, A., Chaabia, N., & Fodil, R. (2020). Improvement of ZnO nanorods photoelectrochemical, optical, structural, and morphological characterizations by cerium ions doping. *Journal of Alloys and Compounds*, 829:154498.
- Abdulrahman, A. F., Ahmed, S. M., & Almessiere, M. A. (2017). Effect of the growth time on the optical properties of ZnO nanorods grown by low temperature method. *Digest Journal of Nanomaterials & Biostructures (DJNB)*, 12(4):1001-1009.
- Acar, C., & Dincer, I. (2015). Impact assessment and efficiency evaluation of hydrogen production methods. *International journal of energy research*, 39(13): 1757- 1768.
- Ahmed, M., & Dincer, I. (2019). A review on photoelectrochemical hydrogen production systems: challenges and future directions. *International Journal of Hydrogen Energy*, 44(5): 2474-2507.
- Akhtar, N., Metkar, S. K., Girigoswami, A., & Girigoswami, K. (2017). ZnO nanoflower based sensitive nano-biosensor for amyloid detection. *Materials Science and Engineering: C*, 78 (1): 960-96.
- Al-Gaashani, R., Radiman, S., Daud, A. R., Tabet, N., & Al-Douri, Y. J. C. I. (2013). XPS and optical studies of different morphologies of ZnO nanostructures prepared by microwave methods. *Ceramics International*, 39(3): 2283-2292.
- Ali, A. S. (2020). Application of Nanomaterials in Environmental Improvement. In *Nanotechnology and the Environment*.(pp. 1-20), Publisher: IntechOpen.
- Alshehri, N. A., Lewis, A. R., Pleydell-Pearce, C., & Maffeis, T. G. (2018). Investigation of the growth parameters of hydrothermal ZnO nanowires for scale up applications. *Journal of Saudi Chemical Society*, 22(5): 538-545.
- Andrews, D., Nann, T., & Lipson, R. H. (2019). *Comprehensive Nanoscience and Nanotechnology*. London, UK. Academic Press.
- Arulraj, A., Ilayaraja, N., Rajeshkumar, V., & Ramesh, M. (2019). Direct Synthesis of cubic shaped Ag₂S on Ni mesh as Binder-free Electrodes for Energy Storage Applications. *Scientific Reports*, 9(1): 1-8.
- Arumugam, J., Raj, A. D., Irudayaraj, A. A., & Thambidurai, M. (2018). Solvothermal synthesis of Bi₂S₃ nanoparticles and nanorods towards solar cell application. *Materials Letters*, 220: 28-31.

- Attanayake, S., Okuya, M., & Murakami, K. (2019). Synthesis and characterization of Al-doped ZnO terrace-truncated nanocone structure by the advanced spray pyrolysis deposition technique. *Japanese Journal of Applied Physics*, 58(8): 080904.
- Badawi, A. (2019). Effect of the non-toxic Ag₂S quantum dots size on their optical properties for environment-friendly applications. *Physica E: Low-dimensional Systems and Nanostructures*, 109:107-113.
- Bagade, C. S., Mali, S. S., Ghanwat, V. B., Khot, K. V., Patil, P. B., Kharade, S. D., Mane, R.M., Desai, N.D., Hong, C.K., Patil, P.S. and Bhosale, P.N. (2015). A facile and low cost strategy to synthesize Cd_{1-x}Zn_xSe thin films for photoelectrochemical performance: effect of zinc content. *RSC Advances*, 5(69): 55658-55668.
- Balachandran, S., & Swaminathan, M. (2013). The simple, template free synthesis of a Bi₂S₃-ZnO heterostructure and its superior photocatalytic activity under UV-A light. *Dalton Transactions*, 42(15): 5338-5347.
- Bao, H., Li, C. M., Cui, X., Gan, Y., Song, Q., & Guo, J. (2008). Synthesis of a highly ordered single - crystalline Bi₂S₃ nanowire array and its metal/semiconductor/metal Back to Back Schottky Diode. *Small*, 4(8):1125-1129.
- Barreto, G. P., Morales, G., & Quintanilla, M. L. L. (2013). Microwave assisted synthesis of ZnO nanoparticles: effect of precursor reagents, temperature, irradiation time, and additives on nano-ZnO morphology development. *Journal of Materials*, 2013:1-11.
- Bera, S., Ghosh, S., & Basu, R. N. (2018). Fabrication of Bi₂S₃/ZnO heterostructures: an excellent photocatalyst for visible-light-driven hydrogen generation and Photoelectrochemical properties. *New Journal of Chemistry*, 42(1): 541-554.
- Bhattacharya, P., Fornari, R., & Kamimura, H. (2011). *Comprehensive Semiconductor Science and Technology*. Italy, Newnes.
- Bora, D. K., & Braun, A. (2014). Solution processed transparent nanoparticulate ZnO thin film electrode for photoelectrochemical water oxidation. *Rsc Advances*, 4(45): 23562-23570.
- Borah, P., Siboh, D., Kalita, P. K., Sarma, J. K., & Nath, N. M. (2018). Quantum confinement induced shift in energy band edges and bandgap of a spherical quantum dot. *Physica B: Condensed Matter*, 530: 208-214.
- Bouroushian, M. (2010). *Electrochemistry of metal chalcogenides*, New York: Springer Science & Business Media.
- Brinker, C. J., & Scherer, G. W. (2013). *Sol-gel science: the physics and chemistry of sol-gel processing*, Boston: Academic press.

- Buhro, W. E., & Colvin, V. L. (2003). Shape matters. *Nature materials*, 2(3): 138-139.
- Cao, Y., Bernechea, M., MacLachlan, A., Zardetto, V., Creatore, M., Haque, S. A., & Konstantatos, G. (2015). Solution processed bismuth sulfide nanowire array core/silver sulfide shell solar cells. *Chemistry of Materials*, 27(10): 3700-3706.
- Chala, S., Sengouga, N., Yakuphanoglu, F., Rahmene, S., Bdirina, M., & Karteri, İ. (2018). Extraction of ZnO thin film parameters for modeling a ZnO/Si solar cell. *Energy*, 164: 871-880.
- Chang, C. H., He, Y., & Pan, C. (2020). Aqueous methods for the synthesis of colloidal metal oxide nanoparticles at ambient pressure. In *Colloidal Metal Oxide Nanoparticles* (pp. 41-66), Publisher: Elsevier.
- Chang, R. (Ed.). (2013). *Surface enhanced Raman scattering*. New York: Springer Science & Business Media.
- Chava, R. K., & Kang, M. (2017). Ag₂S quantum dot sensitized zinc oxide photoanodes for environment friendly photovoltaic devices. *Materials Letters*, 199: 188-191.
- Chen, C., Li, Z., Lin, H., Wang, G., Liao, J., Li, M., Li, S., Lv, & Li, W. (2016). Enhanced visible light photocatalytic performance of ZnO nanowires integrated with CdS and Ag₂S. *Dalton transactions*, 45(9): 3750-3758.
- Chen, H., Wageh, S., Al-Ghamdi, A. A., Wang, H., Yu, J., & Jiang, C. (2019). Hierarchical C/NiO-ZnO nanocomposite fibers with enhanced adsorption capacity for Congo red. *Journal of colloid and interface science*, 537: 736-745.
- Cheng, L., Ding, H., Chen, C., & Wang, N. (2016). Ag₂S/ Bi₂S₃ co-sensitized TiO₂ nanorod arrays prepared on conductive glass as a photoanode for solar cells. *Journal of Materials Science: Materials in Electronics*: 27(4): 3234-3239.
- Choi, H. S., Vaseem, M., Kim, S. G., Im, Y. H., & Hahn, Y. B. (2012). Growth of high aspect ratio ZnO nanorods by solution process: effect of polyethyleneimine. *Journal of Solid State Chemistry*, 189: 25-31.
- Chukwuocha, E. O., Onyeaju, M. C., & Harry, T. S. (2012). Theoretical studies on the effect of confinement on quantum dots using the brus equation. *World Journal of Condensed Matter Physics*, 2: 96-100.
- Coridan, R. H., Nielander, A. C., Francis, S. A., McDowell, M. T., Dix, V., Chatman, S. M., & Lewis, N. S. (2015). Methods for comparing the performance of energy-conversion systems for use in solar fuels and solar electricity generation. *Energy & Environmental Science*, 8(10): 2886-2901.
- Dai Nguyen, T., Man, M. T., Nguyen, M. H., Seo, D. B., & Kim, E. T. (2019). Effect of few-layer MoS₂ flakes deposited ZnO/FTO nanorods on photoelectrochemical characteristic. *Materials Research Express*, 6(8): 085070.

- Dehkordi, H. A., Mokhtari, A., Dastafkan, K., & Soleimanian, V. (2019). Sol–Gel Spin-Coating Followed by Solvothermal Synthesis of Nanorods-Based ZnO Thin Films: Microstructural, Optical, and Gas Sensing Properties. *Journal of Electronic Materials*, 48(2): 1258-1267.
- Desai, M. A., Sharma, V., Prasad, M., Jadkar, S., Saratale, G. D., & Sartale, S. D. (2020). Seed-layer-free deposition of well-oriented ZnO nanorods thin films by SILAR and their photoelectrochemical studies. *International Journal of Hydrogen Energy*, 45(10), 5783-5792.
- Devan, R. S., Patil, R. A., Lin, J. H., & Ma, Y. R. (2012). One- dimensional metal oxide nanostructures: recent developments in synthesis, characterization, and applications. *Advanced Functional Materials*, 22(16): 3326-3370.
- Dolez, P. I. (Ed.). (2015). *Nanoengineering: global approaches to health and safety issues*. Canada. Elsevier.
- Echlin, P., Fiori, C. E., Goldstein, J., Joy, D. C., & Newbury, D. E. (2013). *Advanced scanning electron microscopy and X-ray microanalysis*. New York. Springer Science & Business Media.
- Egerton, R. F. (2005). *Physical principles of electron microscopy: an introduction to TEM, SEM, and AEM*. New York ,Springer Science and Business Media.
- Esparza, D., Zarazúa, I., López-Luke, T., Carriles, R., Torres-Castro, A., & De la Rosa, E. (2015). Photovoltaic properties of Bi₂S₃ and CdS quantum dot sensitized TiO₂ solar cells. *Electrochimica Acta*: 180, 486-492.
- Fang, X., Li, J., Zhao, D., Shen, D., Li, B., & Wang, X. (2009). Phosphorus-doped p-type ZnO nanorods and ZnO nanorod p– n homojunction LED fabricated by hydrothermal method. *The Journal of Physical Chemistry C*, 113(50): 21208-21212.
- Fragalà, M. E., Aleeva, Y., & Malandrino, G. (2011). Effects of Metal-Organic Chemical Vapour Deposition grown seed layer on the fabrication of well aligned ZnO nanorods by Chemical Bath Deposition. *Thin Solid Films*, 519(22):7694-7701.
- Freitas, D.V., González-Moya, J.R., Soares, T.A., Silva, R.R., Oliveira, D.M., Mansur, H.S., Machado, G. and Navarro, M., (2018). Enhanced visible-light photoelectrochemical conversion on TiO₂ nanotubes with Bi₂S₃ quantum dots obtained by in situ electrochemical method. *ACS Applied Energy Materials*, 1(8):3636-3645.
- Gautam, K., Singh, I., Bhatnagar, P. K., & Peta, K. R. (2016). The effect of growth temperature of seed layer on the structural and optical properties of ZnO nanorods. *Superlattices and Microstructures*, 93: 101-108.

- Gerischer, H. (1975). Electrochemical photo and solar cells principles and some experiments. *Journal of Electroanalytical Chemistry and Interfacial Electrochemistry*, 58(1): 263-274.
- Gertman, R., Osherov, A., Golan, Y., & Visoly-Fisher, I. (2014). Chemical bath deposited PbS thin films on ZnO nanowires for photovoltaic applications. *Thin solid films*, 550: 149-155.
- Goldstein, J. I., Newbury, D. E., Michael, J. R., Ritchie, N. W., Scott, J. H. J., & Joy, D. C. (2017). *Scanning electron microscopy and X-ray microanalysis* (4th edition). New York, Springer.
- Gupta, K. M., & Gupta, N. (2016). Semiconductor Materials: Their Properties, Applications, and Recent Advances. In Advanced Semiconducting Materials and Devices (pp. 3-40), Publisher: Springer, Cham.
- Gupta, V., Bhattacharya, P., Yuzuk, Y. I., Sreenivas, K., & Katiyar, R. S. (2006). Optical phonon modes in ZnO nanorods on Si prepared by pulsed laser deposition. *Journal of crystal growth*, 287(1): 39-43.
- Gutiérrez-Lazos, C. D., Fundora-Cruz, A., Solís-Pomar, F., & Pérez-Tijerina, E. (2019). Study of Structural Properties of BiOI on ZnO Thin Films and ZnO Nanorods. *Advances in Materials Science and Engineering*:2019:1-8.
- Han, J., Liu, Z., Yadian, B., Huang, Y., Guo, K., Liu, Z., W., Bo, L., Yajun, & Cui, T. (2014). Synthesis of metal sulfide sensitized zinc oxide-based core/shell/shell nanorods and their photoelectrochemical properties. *Journal of Power Sources*, 268: 388-396.
- Han, M., & Jia, J. (2016). The interlace of Bi₂S₃ nanowires with TiO₂ nanorods: an effective strategy for high photoelectrochemical performance. *Journal of Colloid and Interface Science*, 481: 91-99.
- Hassanpour, A., Bogdan, N., Capobianco, J. A., & Bianucci, P. (2017). Hydrothermal selective growth of low aspect ratio isolated ZnO nanorods. *Materials & Design*, 119: 464-469.
- He, H., Berglund, S. P., Xiao, P., Chemelewski, W. D., Zhang, Y., & Mullins, C. B. (2013). Nanostructured Bi₂S₃ /WO₃ heterojunction films exhibiting enhanced photoelectrochemical performance. *Journal of Materials Chemistry A*, 1(41): 12826-12834.
- Helal, A., Harraz, F. A., Ismail, A. A., Sami, T. M., & Ibrahim, I. A. (2017). Hydrothermal synthesis of novel heterostructured Fe₂O₃/ Bi₂S₃ nanorods with enhanced photocatalytic activity under visible light. *Applied Catalysis B: Environmental*, 213: 18-27.

- Hoang, N. H., & Doan, M. T. (2017). Optimization of an electrode made from CdS–ZnO nanorods for hydrogen generation from photoelectrochemical splitting of water. *Advances in Natural Sciences: Nanoscience and Nanotechnology*, 8(2): 025006.
- Holi, A. M., Zainal, Z., Ayal, A. K., Chang, S. K., Lim, H. N., Talib, Z. A., & Yap, C. C. (2018). Effect of heat treatment on photoelectrochemical performance of hydrothermally synthesised Ag₂S/ZnO nanorods arrays. *Chemical Physics Letters*, 710: 100-107.
- Holi, A. M., Zainal, Z., Ayal, A. K., Chang, S. K., Lim, H. N., Talib, Z. A., & Yap, C. C. (2019). Ag₂S/ZnO Nanorods Composite Photoelectrode Prepared by Hydrothermal Method: Influence of Growth Temperature. *Optik*, 184: 473-479.
- Holi, A. M., Zainal, Z., Talib, Z. A., Lim, H. N., Yap, C. C., Chang, S. K., & Ayal, A. K. (2016). Effect of hydrothermal growth time on ZnO nanorod arrays photoelectrode performance. *Optik*, 127(23): 11111-11118.
- Holi, A. M., Zainal, Z., Talib, Z. A., Lim, H. N., Yap, C. C., Chang, S. K., & Ayal, A. K. (2017). Enhanced photoelectrochemical performance of ZnO nanorod arrays decorated with CdS shell and Ag₂S quantum dots. *Superlattices and Microstructures*, 103: 295-303.
- Hou, T. F., Boppella, R., Shanmugasundaram, A., Kim, D. H., & Lee, D. W. (2017). Hierarchically self-assembled ZnO architectures: establishing light trapping networks for effective photoelectrochemical water splitting. *International Journal of Hydrogen Energy*, 42(22): 15126-15139.
- Hu, W., & Yang, J. (2017). Two-dimensional van der Waals heterojunctions for functional materials and devices. *Journal of Materials Chemistry C*, 5(47):
- Huang, B. R., Chu, J. P., Hsu, C. L., Greene, J. E., Chen, Y. S., & Chang, C. H. (2019). Improving the optical and crystal properties of ZnO nanotubes via a metallic glass quantum dot underlayer. *Journal of Materials Chemistry C*, 7(17): 5163-5171.
- Ihn, T. (2010). *Semiconductor Nanostructures: Quantum states and electronic transport*. New York. Oxford University Press.
- Iqbal, M. Z., & Siddique, S. (2018). Recent progress in efficiency of hydrogen evolution process based photoelectrochemical cell. *International Journal of Hydrogen Energy*, 43(46): 21502-21523.
- Ishikawa, Y., Shimizu, Y., Sasaki, T., & Koshizaki, N. (2006). Preparation of zinc oxide nanorods using pulsed laser ablation in water media at high temperature. *Journal of colloid and interface science*, 300(2): 612-615.
- Islam, M. M., Hasanuzzaman, M., Pandey, A. K., & Rahim, N. A. (2020). Modern energy conversion technologies. In *Energy for Sustainable Development* (pp. 19-39), Publisher: Academic Press.

- Jana, A., Bhattacharya, C., & Datta, J. (2010). Enhanced photoelectrochemical activity of electro-synthesized CdS– Bi₂S₃ composite films grown with self-designed cross-linked structure. *Electrochimica Acta*, 55(22): 6553-6562.
- Jana, A., Bhattacharya, C., Sinha, S., & Datta, J. (2009). Study of the optimal condition for electroplating of Bi₂S₃ thin films and their photoelectrochemical characteristics. *Journal of Solid State Electrochemistry*, 13(9): 1339-1350.
- Jasim, K. E. (2015). Quantum dots solar cells. *Solar Cells-New Approaches and Reviews*. Croatia, Intech Open
- Jiang, C., Moniz, S. J., Wang, A., Zhang, T., & Tang, J. (2017). Photoelectrochemical devices for solar water splitting—materials and challenges. *Chemical Society Reviews*, 46(15): 4645-4660.
- Joy, J., Mathew, J., & George, S. C. (2018). Nanomaterials for photoelectrochemical water splitting—review. *International Journal of Hydrogen Energy*, 43(10): 4804-4817.
- Kaltenhauser, V., Rath, T., Haas, W., Torvisco, A., Müller, S.K., Friedel, B., Kunert, B., Saf, R., Hofer, F. and Trimmel, G., (2013). Bismuth sulphide–polymer nanocomposites from a highly soluble bismuth xanthate precursor. *Journal of Materials Chemistry C*, 1(47): 7825-7832.
- Kamruzzaman, M., & Zapien, J. A. (2017). Synthesis and characterization of ZnO/ZnSe NWs/PbS QDs solar cell. *Journal of Nanoparticle Research*, 19(4):125.
- Khot, K. V., Mali, S. S., Mane, R. M., Patil, P. S., Hong, C. K., Kim, J. H., & Bhosale, P. N. (2015). Synthesis, characterization and photoelectrochemical properties of PbS sensitized vertically aligned ZnO nanorods: modified aqueous route. *Journal of Materials Science: Materials in Electronics*, 26(9), 6897-6906.
- Kilic, B. (2019). Produce of carbon nanotube/ZnO nanowires hybrid photoelectrode for efficient dye-sensitized solar cells. *Journal of Materials Science: Materials in Electronics*, 30(4): 3482-3487.
- Kim, D., & Leem, J. Y. (2018). Effect of the pH of an aqueous solution on the structural, optical, and photoresponse properties of hydrothermally grown ZnO nanorods and the fabrication of a high performance ultraviolet sensor. *Journal of the Korean Physical Society*, 72(3): 400-405.
- Kim, J. S., Kang, B. H., Jeong, H. M., Kim, S. W., Xu, B., & Kang, S. W. (2018). Quantum dot light emitting diodes using size-controlled ZnO NPs. *Current Applied Physics*, 18(6): 681-685.
- Kim, K. S., & Kim, H. W. (2003). Synthesis of ZnO nanorod on bare Si substrate using metal organic chemical vapor deposition. *Physica B: Condensed Matter*, 328(3-4): 368-371.

- Kokane, S. K., Supekar, A. T., Baviskar, P. K., Palve, B. M., Jadkar, S. R., Mohite, K. C., & Pathan, H. M. (2018). CdS sensitized pristine and Cd doped ZnO solar cells: Effect of SILAR cycles on optical properties and efficiency. *Materials Science in Semiconductor Processing*, 80: 179-183.
- Konstantatos, G., Levina, L., Tang, J., & Sargent, E. H. (2008). Sensitive solution-processed Bi₂S₃ nanocrystalline photodetectors. *Nano letters*, 8(11):4002-4006.
- Kumar, D., Bai, R., Chaudhary, S., & Pandya, D. K. (2017). Enhanced photoelectrochemical response for hydrogen generation in self-assembled aligned ZnO/PbS core/shell nanorod arrays grown by chemical bath deposition. *Materials today energy*, 6: 105-114.
- Kumar, S., Sharma, S., Sood, S., Umar, A., & Kansal, S. K. (2016). Bismuth sulfide (Bi₂S₃) nanotubes decorated TiO₂ nanoparticles heterojunction assembly for enhanced solar light driven photocatalytic activity. *Ceramics International*, 42(15): 17551-17557.
- Kumar, S., Sharma, S., Umar, A., & Kansal, S. K. (2016). Bismuth sulphide (Bi₂S₃) nanotubes as an efficient photocatalyst for methylene blue dye degradation. *Nanoscience and Nanotechnology Letters*, 8(3): 266-272.
- Kuo, S. Y., Chen, W. C., Lai, F. I., Cheng, C. P., Kuo, H. C., Wang, S. C., & Hsieh, W. F. (2006). Effects of doping concentration and annealing temperature on properties of highly-oriented Al-doped ZnO films. *Journal of Crystal Growth*, 287(1): 78-84.
- Kurudirek, S. V., Menkara, H., Klein, B. D., Hertel, N. E., & Summers, C. J. (2018). Effect of annealing temperature on the photoluminescence and scintillation properties of ZnO nanorods. Nuclear Instruments and Methods in Physics Research Section A: Accelerators, Spectrometers, Detectors and Associated Equipment, 877: 80-86.
- Kyono, A., & Kimata, M. (2004). Structural variations induced by difference of the inert pair effect in the stibnite-bismuthinite solid solution series (Sb, Bi)₂S₃. *American Mineralogist*, 89(7): 932-940.
- Lee, W., Min, S. K., Dhas, V., Ogale, S. B., & Han, S. H. (2009). Chemical bath deposition of CdS quantum dots on vertically aligned ZnO nanorods for quantum dots-sensitized solar cells. *Electrochemistry Communications*, 11(1): 103-106.
- Li, C., Zhao, J., Hu, Q., Liu, Z., Yu, Z., & Yan, H. (2016). Crystal structure and transporting properties of Bi₂S₃ under high pressure: Experimental and theoretical studies. *Journal of Alloys and Compounds*, 688: 329-335.
- Li, D., Ma, J., Zhou, L., Li, Y., & Zou, C. (2015). Synthesis and characterization of Cu₂S nanoparticles by diethylenetriamine-assisted hydrothermal method. *Optik*, 126(24): 4971-4973.

- Li, W., Yang, J., Jiang, Q., Luo, Y., Hou, Y., Zhou, S., Xiao, Y., Fu, L. and Zhou, Z., (2016). Electrochemical atomic layer deposition of Bi_2S_3 / Sb_2S_3 quantum dots co-sensitized TiO_2 nanorods solar cells. *Journal of Power Sources*, 307:690-696.
- Li, X., Li, J., Cui, C., Liu, Z., & Niu, Y. (2016). PbS nanoparticle sensitized ZnO nanowire arrays to enhance photocurrent for water splitting. *The Journal of Physical Chemistry C*, 120(8): 4183-4188.
- Li, Z., Luo, W., Zhang, M., Feng, J., & Zou, Z. (2013). Photoelectrochemical cells for solar hydrogen production: current state of promising photoelectrodes, methods to improve their properties, and outlook. *Energy & Environmental Science*, 6(2):347-370.
- Liang, Z., Zhang, Q., Wiranwetchayan, O., Xi, J., Yang, Z., Park, K., Li, C. & Cao, G. (2012). Effects of the morphology of a ZnO buffer layer on the photovoltaic performance of inverted polymer solar cells. *Advanced Functional Materials*, 22(10): 2194-2201.
- Lin, Y. C., & Lee, M. W. (2014). Bi_2S_3 liquid-junction semiconductor-sensitized SnO_2 solar cells. *Journal of The Electrochemical Society*, 161(1): H1-H5.
- Liu, C., Liu, Z., Li, Y., Ya, J., Lei, E., & An, L. (2011). CdS/PbS co-sensitized ZnO nanorods and its photovoltaic properties. *Applied surface science*, 257(16), 7041-7046.
- Liu, C., Yang, Y., Li, W., Li, J., Li, Y., & Chen, Q. (2016). A novel Bi_2S_3 nanowire@ TiO_2 nanorod heterogeneous nanostructure for photoelectrochemical hydrogen generation. *Chemical Engineering Journal*, 302, 717-724.
- Liu, N., Albu, S. P., Lee, K., So, S., & Schmuki, P. (2012). Water annealing and other low temperature treatments of anodic TiO_2 nanotubes: A comparison of properties and efficiencies in dye sensitized solar cells and for water splitting. *Electrochimica acta*, 82: 98-102.
- Liu, S., Wang, X., Zhao, W., Wang, K., Sang, H., & He, Z. (2013). Synthesis, characterization, and enhanced photocatalytic performance of Ag_2S -coupled ZnO/ZnS core/shell nanorods. *Journal of Alloys and Compounds*, 568:84-91.
- Liu, X., Wu, X., Cao, H., & Chang, R. P. (2004). Growth mechanism and properties of ZnO nanorods synthesized by plasma-enhanced chemical vapor deposition. *Journal of Applied Physics*, 95(6): 3141-3147.
- Louër, D., & Audebrand, N. (1999). Profile fitting and diffraction line broadening analysis. *Advances in X-ray Analysis*, 41: 556-565.
- Lu, J. G., Chang, P., & Fan, Z. (2006). Quasi-one-dimensional metal oxide materials Synthesis, properties, and applications. *Materials Science and Engineering: R: Reports*, 52(1-3): 49-91

- Luo, C.Q., Ling, F.C.C., Rahman, M.A., Phillips, M., Ton-That, C., Liao, C., Shih, K., Lin, J., Tam, H.W., Djurišić, A.B. and Wang, S.P., (2019). Surface polarity control in ZnO films deposited by pulsed laser deposition. *Applied Surface Science*, 483 :1129-1135.
- Ma, A., Wei, Y., Zhou, Z., Xu, W., Ren, F., Ma, H., & Wang, J. (2012). Preparation Bi₂S₃ –TiO₂ heterojunction/polymer fiber composites and its photocatalytic degradation of methylene blue under Xe lamp irradiation. *Polymer Degradation and Stability*, 97(2): 125-131.
- Mageshwari, K., & Sathyamoorthy, R. (2013). Nanocrystalline Bi₂S₃ thin films grown by thio-glycolic acid mediated successive ionic layer adsorption and reaction (SILAR) technique. *Materials Science in Semiconductor Processing*, 16(1) : 43-50.
- Mahapatra, A. D., & Basak, D. (2019). Enhanced ultraviolet photosensing properties in Bi₂S₃ nanoparticles decorated ZnO nanorods' heterostructure. *Journal of Alloys and Compounds*, 797: 766-774.
- Majumder, T., Dhar, S., Chakraborty, P., Debnath, K., & Mondal, S. P. (2018). Advantages of ZnO nanotaper photoanodes in photoelectrochemical cells and graphene quantum dot sensitized solar cell applications. *Journal of Electroanalytical Chemistry*, 813: 92-101.
- Manassen, J., Cahen, D., Hodes, G., & Sofer, A. (1976). Electrochemical, solid state, photochemical and technological aspects of photoelectrochemical energy converters. *Nature*, 263(5573): 97-100.
- Mane, R. S., & Lokhande, C. D. (2000). Chemical deposition method for metal chalcogenide thin films. *Materials Chemistry and Physics*, 65(1):1-31.
- Messaoudi, O., Makhlof, H., Souissi, A., Amiri, G., Bardaoui, A., Oueslati, M., Bechelany, M. and Chtourou, R., (2015). Synthesis and characterization of ZnO/Cu₂O core–shell nanowires grown by two-step electrodeposition method. *Applied Surface Science*, 343:148-152.
- Miao, J., & Liu, B. (2015). II–VI semiconductor nanowires: ZnO. In *Semiconductor Nanowires* (pp. 3-28), Publisher: Woodhead Publishing.
- Minceva-Sukarova, B., Najdoski, M., Grozdanov, I., & Chunnillall, C. J. (1997). Raman spectra of thin solid films of some metal sulfides. *Journal of Molecular Structure*, 410: 267-270.
- Mishra, P. K., & Tiwari, P. (2020). Solar Photovoltaic Technology—A Review. *Advanced Science, Engineering and Medicine*, 12(1): 5-10.
- Mohd Fudzi, L., Zainal, Z., Lim, H. N., Chang, S. K., & Holi, A. M. (2018). Effect of temperature and growth time on vertically aligned ZnO nanorods by simplified hydrothermal technique for photoelectrochemical cells. *Materials*, 11(5):704.

- Mourad, S., El Ghoul, J., Omri, K., & Khirouni, K. (2019). Indium doping effect on properties of ZnO nanoparticles synthesized by sol–gel method. *Chinese Physics B*, 28(4): 047701.
- Müller, M. O., Stämpfli, A., Dold, U., & Hammer, T. (2011). Energy autarky: A conceptual framework for sustainable regional development. *Energy policy*, 39(10): 5800-5810.
- Murillo, G., Lozano, H., Cases-Utrera, J., Lee, M., & Esteve, J. (2017). Improving Morphological Quality and Uniformity of Hydrothermally Grown ZnO Nanowires by Surface Activation of Catalyst Layer. *Nanoscale Research Letters*, 12(1): 1-8.
- Narayanan, G. N., Ganesh, R. S., & Karthigeyan, A. (2016). Effect of annealing temperature on structural, optical, and electrical properties of hydrothermal assisted zinc oxide nanorods. *Thin Solid Films*, 598: 39-45.
- Nasirpouri, F. (2017). Fundamentals and principles of electrode-position. In Electrodeposition of nanostructured materials (pp. 75-121), Publisher: Springer, Cham.
- Nesheva, D., Dzhurkov, V., Stambolova, I., Blaskov, V., Bineva, I., Moreno, J.M.C., Preda, S., Gartner, M., Hristova-Vasileva, T. and Shipochka, M., (2018). Surface modification and chemical sensitivity of sol gel deposited nanocrystalline ZnO films. *Materials Chemistry and Physics*, 209:165-171.
- Nguyen, O., Krins, N., & Laberty-Robert, C. (2018). Harvesting light with semiconductor: Role of interface in the processes of charge transfer. *Materials Science in Semiconductor Processing*, 73: 2-12.
- Nikam, P. R., Baviskar, P. K., Majumder, S., Sali, J. V., & Sankapal, B. R. (2018). SILAR controlled CdSe nanoparticles sensitized ZnO nanorods photoanode for solar cell application: electrolyte effect. *Journal of Colloid and Interface Science*, 524: 148-155.
- Nikam, P. R., Baviskar, P. K., Sali, J. V., Gurav, K. V., Kim, J. H., & Sankapal, B. R. (2015). SILAR coated Bi₂S₃ nanoparticles on vertically aligned ZnO nanorods: Synthesis and characterizations. *Ceramics International*, 41(9): 10394-10399.
- Nikam, P. R., Baviskar, P. K., Sali, J. V., Gurav, K. V., Kim, J. H., & Sankapal, B. R. (2016). CdS surface encapsulated ZnO nanorods: Synthesis to solar cell application. *Journal of Alloys and Compounds*, 689: 394-400.
- Norton, D. P., Heo, Y. W., Ivill, M. P., Ip, K., Pearton, S. J., Chisholm, M. F., & Steiner, T. (2004). ZnO: growth, doping & processing. *Materials Today*, 7(6): 34-40.
- Nunes, D., Pimentel, A., Santos, L., Barquinha, P., Pereira, L., Fortunato, E., & Martins, R. (2018). *Metal Oxide Nanostructures: Synthesis, Properties and Applications*. Chennai, Elsevier.

- Ong, C. B., Ng, L. Y., & Mohammad, A. W. (2018). A review of ZnO nanoparticles as solar photocatalysts: synthesis, mechanisms, and applications. *Renewable and Sustainable Energy Reviews*, 81: 536-551.
- Özgür, Ü., Avrutin, V., & Morkoç, H. (2018). Zinc Oxide Materials and Devices Grown by Molecular Beam Epitaxy. In *Molecular Beam Epitaxy* (pp. 343-375), Publisher: Elsevier.
- Ozgur, U., Hofstetter, D., & Morkoc, H. (2010). ZnO devices and applications: a review of current status and future prospects. *Proceedings of the IEEE*, 98(7): 1255-1268.
- Palit, S., & Hussain, C. M. (2020). Green Nanomaterials: A Sustainable Perspective. In *Green Nanomaterials* (pp. 23-41). Publisher: Springer.
- Pandit, B., Sharma, G. K., & Sankapal, B. R. (2017). Chemically deposited Bi₂S₃ : PbS solid solution thin film as supercapacitive electrode. *Journal of Colloid and Interface Science*, 505: 1011-1017.
- Pankove, J. I. (1975). *Optical processes in semiconductors*. New York. Courier Corporation.
- Parize, R., Garnier, J., Chaix-Pluchery, O., Verrier, C., Appert, E., & Consonni, V. (2016). Effects of hexamethylenetetramine on the nucleation and radial growth of ZnO nanowires by chemical bath deposition. *The Journal of Physical Chemistry C*, 120(9): 5242-5250.
- Park, J. Y., Lee, D. J., & Kim, S. S. (2005). Size control of ZnO nanorod arrays grown by metalorganic chemical vapour deposition. *Nanotechnology*, 16(10):2044.
- Parkinson, B., Turner, J., Peter, L., Lewis, N., Sivula, K., Domen, K., Bard, A.J., Fiechter, S., Collazo, R., Hannappel, T. and Hellman, A. (2013). *Photoelectrochemical water splitting: materials, processes, and architectures*. Royal Society of Chemistry.
- Pathan, H. M., & Lokhande, C. D. (2004). Deposition of metal chalcogenide thin films by successive ionic layer adsorption and reaction (SILAR) method. *Bulletin of Materials Science*, 27(2): 85-111.
- Patil, S. A., Hwang, Y. T., Jadhav, V. V., Kim, K. H., & Kim, H. S. (2017). Solution processed growth and photoelectrochemistry of Bi₂S₃ nanorods thin film. *Journal of Photochemistry and Photobiology A: Chemistry*, 332:174-181.
- Pawar, S. A., Patil, D. S., Kim, J. H., Patil, P. S., & Shin, J. C. (2017). Quantum dot sensitized solar cell based on TiO₂/CdS/Ag₂S heterostructure. *Optical Materials*, 66: 644-650.
- Pellicano, C. M., & Yanagi, H. (2020). Accelerated growth of nanostructured ZnO films via low temperature microwave-assisted H₂O oxidation for solar cell applications. *Applied Surface Science*, 506: 144917.

- Pineda, E., Nicho, M. E., Nair, P. K., & Hu, H. (2012). Optoelectronic properties of chemically deposited Bi_2S_3 thin films and the photovoltaic performance of $\text{Bi}_2\text{S}_3/\text{P}_3\text{OT}$ solar cells. *Solar Energy*, 86(4): 1017-1022.
- Pourshaban, E., Abdizadeh, H., & Golobostanfard, M. R. (2015). ZnO nanorods array synthesized by chemical bath deposition: effect of seed layer sol concentration. *Procedia Materials Science*, 11: 352-358.
- Qiu, W. T., Huang, Y. C., Wang, Z. L., Xiao, S., Ji, H. B., & Tong, Y. X. (2017). Effective strategies towards high-performance photoanodes for photoelectrochemical water splitting. *Acta Physico-Chimica Sinica*, 33(1): 80-102.
- Qu, X., Lü, S., Wang, J., Li, Z., & Xue, H. (2012). Preparation and optical property of porous ZnO nanobelts. *Materials Science in Semiconductor Processing*, 15(3): 244-250.
- Rajeshwar, K., Singh, P., & DuBow, J. (1978). Energy conversion in photoelectrochemical systems—a review. *Electrochimica Acta*, 23(11): 1117-1144.
- Rama Krishna, M. V., & Friesner, R. A. (1991). Quantum confinement effects in semiconductor clusters. *The Journal of Chemical Physics*, 95(11): 8309-8322.
- Rattanawarinchai, P., Khemasiri, N., Jessadaluk, S., Chananonnawathorn, C., Horprathum, M., Klamchuen, A., Kayunkid, N., Rahong, S., Phromyothin, D. and Nukeaw, J., (2018). Growth Time Dependence on Photoelectrochemical Property of Zinc Oxide Nanorods Prepared by Hydrothermal Synthesis. *Surface Review and Letters*, 25(Supp01):1840001.
- Raut, H. K., Ganesh, V. A., Nair, A. S., & Ramakrishna, S. (2011). Anti-reflective coatings: A critical, in-depth review. *Energy & Environmental Science*, 4(10): 3779-3804.
- Raut, S. S., Dhobale, J. A., & Sankapal, B. R. (2017). SILAR deposited Bi_2S_3 thin film towards electrochemical supercapacitor. *Physica E: Low-dimensional Systems and Nanostructures*, 87: 209-212
- Rodnyi, P. A., & Khodyuk, I. V. (2011). Optical and luminescence properties of zinc oxide. *Optics and Spectroscopy*, 111(5): 776-785.
- Sadovnikov, S. I., Gusev, A. I., & Rempel, A. A. (2015). Artificial silver sulfide Ag_2S : crystal structure and particle size in deposited powders. *Superlattices and Microstructures*, 83: 35-47.
- Saha, J.K., Billah, M.M., Bukke, R.N., Kim, Y.G., Mude, N.N., Siddik, A.B., Islam, M.M., Do, Y., Choi, M. and Jang, J., (2020). Highly Stable, Nanocrystalline, ZnO Thin-Film Transistor by Spray Pyrolysis Using High-K Dielectric. *IEEE Transactions on Electron Devices*, 67(3): 1021-1026.

- Sakano, T., Tanaka, Y., Nishimura, R., Nedyalkov, N. N., Atanasov, P. A., Saiki, T., & Obara, M. (2008). Surface enhanced Raman scattering properties using Au-coated ZnO nanorods grown by two-step, off-axis pulsed laser deposition. *Journal of Physics D: Applied Physics*, 41(23): 235304.
- Saleem, M., Fang, L., Ruan, H. B., Wu, F., Huang, Q. L., Xu, C. L., & Kong, C. Y. (2012). Effect of zinc acetate concentration on the structural and optical properties of ZnO thin films deposited by Sol-Gel method. *International Journal of Physical Sciences*, 7(23): 2971-2979.
- Salunkhe, D. B., Dubal, D. P., Sali, J. V., & Sankapal, B. R. (2015). Linker free synthesis of TiO₂/Bi₂S₃ heterostructure towards solar cell application: Facile chemical routes. *Materials Science in Semiconductor Processing*, 30: 335-342.
- Sanjeev, S., & Kekuda, D. (2015). Effect of annealing temperature on the structural and optical properties of zinc oxide (ZnO) thin films prepared by spin coating process. In IOP Conference Series: *Materials Science and Engineering* 73(1): 012149. IOP Publishing.
- Schneller, T., Waser, R., Kos, M., & Payne, D. (Eds.). (2013). *Chemical solution deposition of functional oxide thin films*. Vienna. Springer Vienna.
- Seah, M. P., & Dench, W. A. (1979). Quantitative electron spectroscopy of surfaces: A standard data base for electron inelastic mean free paths in solids. *Surface and Interface Analysis*, 1(1): 2-11.
- Seipel, B., Nadarajah, A., Wutzke, B., & Könenkamp, R. (2009). Electrodeposition of ZnO nanorods in the presence of metal ions. *Materials Letters*, 63(9-10): 736-738.
- Shahzad, N., Shah, Z., Shahzad, M. I., Ahmad, K., & Pugliese, D. (2019). Effect of seed layer on the performance of ZnO nanorods-based photoanodes for dye-sensitized solar cells. *Materials Research Express*, 6(10):105523.
- Shi, B., Qi, Y., & Tian, L. (2020). Fabrication of Ag₂S quantum dots sensitized CdSe photoelectrodes and its photoelectric performance. *Materials Chemistry and Physics*, 240: 122177.
- Sindhu, H. S., Joishy, S., Rajendra, B. V., Rao, A., Gaonkar, M., Kulkarni, S. D., & Babu, P. D. (2017). Materials Science in Semiconductor Processing Tuning optical, electrical, and magnetic properties of fiber structured ZnO film by deposition temperature and precursor concentration. *Materials Science in Semiconductor Processing*, 68: 97-107.
- Singh, R. (2002). CV Raman and the Discovery of the Raman Effect. *Physics in Perspective*, 4(4): 399-420.
- Solís, M., Rincón, M. E., Calva, J. C., & Alvarado, G. (2013). Bismuth sulfide sensitized TiO₂ arrays for photovoltaic applications. *Electrochimica Acta*, 112:159-163.

- Solís-Pomar, F., Martínez, E., Meléndrez, M. F., & Pérez-Tijerina, E. (2011). Growth of vertically aligned ZnO nanorods using textured ZnO films. *Nanoscale Research Letters*, 6(1): 524.
- Song, X., Liu, Z., Tian, T., Ma, Z., Yan, Y., Li, X., Dong, X., Wang, Y. and Xia, C., (2019). Lead sulfide films synthesized by microwave-assisted chemical bath deposition method as efficient counter electrodes for CdS/CdSe sensitized ZnO nanorod solar cells. *Solar Energy*, 177: 672-678.
- Suchea, M., Christoulakis, S., Moschovis, K., Katsarakis, N., & Kiriakidis, G. (2006). ZnO transparent thin films for gas sensor applications. *Thin solid films*, 515(2): 551-554.
- Suma, M. N., Prasad, M. V. N., Gaddam, V., Rajanna, K., & Nayak, M. M. (2019). Development of a Novel Acoustic Sensor using Sputtered ZnO Thin Film. *Journal of Pure Applied and Industrial Physics*, 9(1): 1-7.
- Sun, Y., Fuge, G. M., & Ashfold, M. N. (2004). Growth of aligned ZnO nanorod arrays by catalyst-free pulsed laser deposition methods. *Chemical Physics Letters*, 396(1-3): 21-26.
- Sun, Y., Riley, D. J., & Ashfold, M. N. (2006). Mechanism of ZnO nanotube growth by hydrothermal methods on ZnO film-coated Si substrates. *The Journal of Physical Chemistry B*, 110(31): 15186-15192.
- Tahir, A. A., Ehsan, M. A., Mazhar, M., Wijayantha, K. U., Zeller, M., & Hunter, A. D. (2010). Photoelectrochemical and photoresponsive properties of Bi₂S₃ nanotube and nanoparticle thin films. *Chemistry of Materials*, 22(17): 5084-5092.
- Tang, C., Wang, C., Su, F., Zang, C., Yang, Y., Zong, Z., & Zhang, Y. (2010). Controlled synthesis of urchin-like Bi₂S₃ via hydrothermal method. *Solid State Sciences*, 12(8): 1352-1356.
- Tang, C., Zhang, Y., Su, J., Wang, C., Sun, R., Zhang, J., & Li, G. (2016). Synthesis and photocatalytic properties of vertically aligned Bi₂S₃ platelets. *Solid State Sciences*, 51: 24-29.
- Tauc, J., Grigorovici, R., & Vancu, A. (1966). Optical properties and electronic structure of amorphous germanium. *Physica Status Solidi (b)*, 15(2): 627-637.
- Terasako, T., Obara, S., Yagi, M., Nomoto, J., & Yamamoto, T. (2019). Structural and photoluminescence properties of ZnO nanorods grown on ion-plated Ga-doped ZnO seed layers by chemical bath deposition and fabrication of poly (3, 4-ethylenedioxythiophene) poly (styrenesulfonate)/ZnO nanorods heterostructures. *Thin Solid Films*, 677: 109-118.
- Tharsika, T., Thanihaichelvan, M., Haseeb, A. S. M. A., & Akbar, S. A. (2019). Highly Sensitive and Selective Ethanol Sensor Based on ZnO Nanorod on SnO₂ Thin Film Fabricated by Spray Pyrolysis. *Frontiers in Materials*. 6:122.

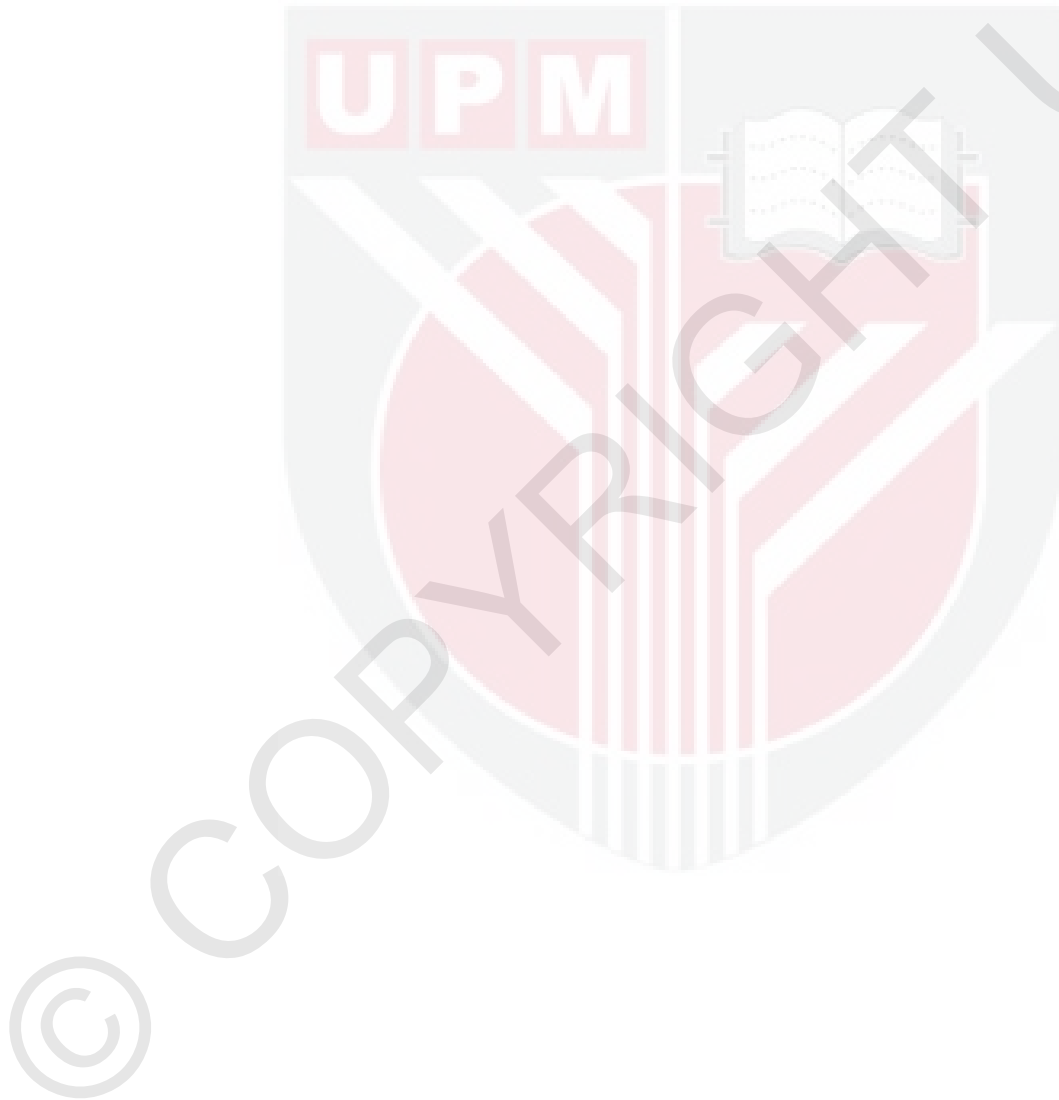
- Tien, L. C., Norton, D. P., Pearton, S. J., Wang, H. T., & Ren, F. (2007). Nucleation control for ZnO nanorods grown by catalyst-driven molecular beam epitaxy. *Applied Surface Science*, 253(10): 4620-4625.
- Tripathi, S., Agarwal, R., & Singh, D. (2019). Size Dependent Elastic and Thermophysical Properties of ZnO Nanowires. *Johnson Matthey Technology Review*. 63(3): 166–176.
- Truong, N.H., Van Nguyen, T., Pham, T.A.T., Van Hoang, D., Vu, H.M., Nguyen, H.C., Phan, T.B. and Tran, V.C., (2019). Influence of indium and hydrogen co-doping on optical and electrical properties of zinc oxide thin films deposited by DC magnetron sputtering. *Science and Technology Development Journal*, 22(2): 253-257.
- Van de Krol, R., & Grätzel, M. (2012). *Photoelectrochemical hydrogen production* (Vol. 90). New York: Springer.
- Varghese, R. J., Parani, S., Thomas, S., Oluwafemi, O. S., & Wu, J. (2019). Introduction to nanomaterials: synthesis and applications. In *Nanomaterials for Solar Cell Applications* (pp. 75-95). Elsevier.
- Vattikuti, S. P. (2018). Heterostructured Nanomaterials: Latest Trends in Formation of Inorganic Heterostructures. In *Synthesis of Inorganic Nanomaterials* (pp. 89-120). Woodhead Publishing.
- Velanganni, S., Manikandan, A., Prince, J. J., Mohan, C. N., & Thiruneelakandan, R. (2018). Nanostructured ZnO coated Bi₂S₃ thin films: Enhanced photocatalytic degradation of methylene blue dye. *Physica B: Condensed Matter*, 545: 383-389.
- Wan, Y., Han, M., Yu, L., Yi, G., & Jia, J. (2016). 3D Bi₂S₃ salix leaf-like nanosheet/TiO₂ nanorod branched heterostructure arrays for improving photoelectrochemical properties. *CrystEngComm*, 18(9): 1577-1584.
- Wang, C., Zhang, X., Wang, D., Yang, Z., Ji, W., Zhang, C., & Zhao, Y. (2010). Synthesis of nanostructural ZnO using hydrothermal method for dye-sensitized solar cells. *Science China Technological Sciences*, 53(4): 1146-1149.
- Wang, F., Song, L., Zhang, H., Luo, L., Wang, D., & Tang, J. (2017). One-dimensional metal-oxide nanostructures for solar photocatalytic water-splitting. *Journal of Electronic Materials*, 46(8): 4716-4724.
- Wang, G., Li, M., Chen, C., Lv, S., Liao, J., & Li, Z. (2016). Enhanced field emission properties of ZnO–Ag₂S core–shell heterojunction nanowires. *Dalton Transactions*, 45(21): 8777-8782.
- Wang, L., Zhang, X., Zhao, S., Zhou, G., Zhou, Y., & Qi, J. (2005). Synthesis of well-aligned ZnO nanowires by simple physical vapor deposition on c-oriented ZnO thin films without catalysts or additives. *Applied Physics Letters*, 86(2): 024108.

- Wang, L., Zhao, D., Su, Z., & Shen, D. (2012). Hybrid polymer/ZnO solar cells sensitized by PbS quantum dots. *Nanoscale Research Letters*, 7(1): 106.
- Wang, Y., Chen, J., Jiang, L., Sun, K., Liu, F., & Lai, Y. (2016). Photoelectrochemical properties of Bi₂S₃ thin films deposited by successive ionic layer adsorption and reaction (SILAR) method. *Journal of Alloys and Compounds*, 686: 684-692.
- Wang, Z., Luo, C., Anwand, W., Wagner, A., Butterling, M., Rahman, M.A., Phillips, M.R., Ton-That, C., Younas, M., Su, S. and Ling, F.C.C., (2019). Vacancy cluster in ZnO films grown by pulsed laser deposition. *Scientific Reports*, 9(1):1-10.
- Weisbuch, C., & Vinter, B. (2014). *Quantum semiconductor structures: fundamentals and applications*. Boston. Elsevier.
- Wise, F. W. (2000). Lead salt quantum dots: the limit of strong quantum confinement. *Accounts of Chemical Research*, 33(11): 773-780.
- Worasawat, S., Masuzawa, T., Hatanaka, Y., Neo, Y., Mimura, H., & Pecharapa, W. (2018). Synthesis and characterization of ZnO nanorods by hydrothermal method. *Materials Today: Proceedings*, 5(5): 10964-10969.
- Wu, M., Chen, W. J., Shen, Y. H., Huang, F. Z., Li, C. H., & Li, S. K. (2014). In situ growth of matchlike ZnO/Au plasmonic heterostructure for enhanced photoelectrochemical water splitting. *ACS applied materials & interfaces*, 6(17): 15052-15060.
- Xu, S., & Wang, Z. L. (2011). One-dimensional ZnO nanostructures: solution growth and functional properties. *Nano Research*, 4(11):1013-1098.
- Xu, Y., Li, H., Sun, B., Qiao, P., Ren, L., Tian, G., Jiang, B., Pan, K. and Zhou, W., (2020). Surface oxygen vacancy defect-promoted electron-hole separation for porous defective ZnO hexagonal plates and enhanced solar-driven photocatalytic performance. *Chemical Engineering Journal*, 379:122295.
- Xue, J., Liu, J., Mao, S., Wang, Y., Shen, W., Wang, W., Huang, L., Li, H. and Tang, J., (2018). Recent progress in synthetic methods and applications in solar cells of Ag₂S quantum dots. *Materials Research Bulletin*, 106: 113-123.
- Yang, T., Tang, Y.A., Liu, L., Lv, X., Wang, Q., Ke, H., Deng, Y., Yang, H., Yang, X., Liu, G. and Zhao, Y., (2017). Size-dependent Ag₂S nanodots for sond near-infrared fluorescence/photoacoustics imaging and simultaneous photothermal therapy. *ACS Nano*, 11(2): 1848-1857.
- Yang, X., Hu, L., Deng, H., Qiao, K., Hu, C., Liu, Z., Yuan, S., Khan, J., Li, D., Tang, J. and Song, H., (2017). Improving the performance of PbS quantum dot solar cells by optimizing ZnO window layer. *Nano-micro Letters*, 9(2): 24.

- Yang, X., Tian, S., Li, R., Wang, W., & Zhou, S. (2017). Use of single-crystalline Bi_2S_3 nanowires as room temperature ethanol sensor synthesized by hydrothermal approach. *Sensors and Actuators B: Chemical*, 241:210-216.
- Yao, K., Gong, W. W., Hu, Y. F., Liang, X. L., Chen, Q., & Peng, L. M. (2008). Individual Bi_2S_3 nanowire-based room-temperature H_2 sensor. *The Journal of Physical Chemistry C*, 112(23): 8721-8724.
- Yilmaz, C., & Unal, U. (2015). Photoelectrochemical properties of electrochemically deposited metal chalcogenide/ZnO films. *Applied Surface Science*, 350:87-93.
- Yin, Z., Wu, S., Zhou, X., Huang, X., Zhang, Q., Boey, F., & Zhang, H. (2010). Electrochemical deposition of ZnO nanorods on transparent reduced graphene oxide electrodes for hybrid solar cells. *Small*, 6(2), 307-312.
- Yoffe, A. D. (1993). Low-dimensional systems: quantum size effects and electronic properties of semiconductor microcrystallites (zero-dimensional systems) and some quasi-two-dimensional systems. *Advances in Physics*, 42(2):173-262.
- Zak, A. K., Abrishami, M. E., Majid, W. A., Yousefi, R., & Hosseini, S. M. (2011). Effects of annealing temperature on some structural and optical properties of ZnO nanoparticles prepared by a modified sol-gel combustion method. *Ceramics International*, 37(1): 393-398.
- Zhang, Y., Feng, T., Zhou, X., Pei, Q., Hao, T., Zhang, W., Wu, S., Mao, H. and Song, X.M., (2016). Facile preparation of one dimension ZnO/chalcogenide semiconductor heterostructure for efficient photoelectrochemical water splitting. *Journal of Alloys and Compounds*, 685: 581-586.
- Zhao, G., Sun, M., Liu, X., Xuan, J., Kong, W., Zhang, R., Sun, Y., Jia, F., Yin, G. and Liu, B., (2019). Fabrication of CdS quantum dots sensitized ZnO nanorods/ TiO_2 nanosheets hierarchical heterostructure films for enhanced photoelectrochemical performance. *Electrochimica Acta*, 304: 334-341.
- Znaidi, L. (2010). Sol-gel-deposited ZnO thin films: A review. *Materials Science and Engineering: B*, 174(1-3): 18-30.
- Zumeta-Dube, I., Ruiz-Ruiz, V. F., Diaz, D., Rodil-Posadas, S., & Zeinert, A. (2014). TiO_2 sensitization with Bi_2S_3 quantum dots: the inconvenience of sodium ions in the deposition procedure. *The Journal of Physical Chemistry C*, 118(22):11495-11504.

BIODATA OF STUDENT

The student, Asla Abdullah Al-Zahrani was born on May 15th, 1980 in Al-Bahah, Saudi Arabia. She joined AL-Bahah University in 1999 and received her bachelor's degree in Chemistry from AL-Bahah University, in 2003. In 2004, she joined AL-Bahah University as a teaching assistant. She obtained her M. Sc. in Physical Chemistry from Imam Abdulrahman Bin Faisal University in 2013. Since 2009 up to now, she works as lecturer in the Department of chemistry, Science college, Imam Abdulrahman Bin Faisal University in eastern region, Dammam, Saudi Arabia. In 2017, she enrolled as a full-time PhD degree in Physical Chemistry at Universiti Putra Malaysia, under scholarship of the Saudi culture mission and Imam Abdulrahman Bin Faisal University.



LIST OF PUBLICATIONS

- Al-Zahrani, A. A., Zainal, Z., Talib, Z. A., Lim, H. N., Fudzi, L. M., Holi, A. M., ... & Sarif, M. Effect of Annealing Temperature on the Performance of ZnO Seed Layer for Photoanode in Photoelectrochemical Cells. *Defect and Diffusion Forum* (2020) 398: 156-166. (Q3/IF 2019=0.66). Publisher: Trans Tech Publications Ltd.
- Al-Zahrani, A. A., Zulkarnain Zainal, Zainal Abidin Talib, Janet Lim Hong Ngee, Laimy Mohd Fudzi, Araa Mebdir Holi and Mahanim Sarif @Mohd Ali 'Effect of hydrothermal growth temperature and time on physical properties and photoanode performance of ZnO Nanorods", *International Journal of Nanoelectronics and Materials*,(2020) 13(2): 341-360.(Q3/IF 2018=0.88). Publisher:Universiti Malaysia Peerlis (UniMAP).
- AL-Zahrani, A. A., Zainal, Z., Talib, Z. A., Lim, H. N., Mohd Fudzi, L., & Holi, A. M. Synthesis of Binary Bi₂S₃/ZnO Nanorod Array Heterostructure and Their Photoelectrochemical Performance. *Journal of Nanomaterials*, (2019)2019: 1-10. (Q2/IF 2019= 2.233). Puplisher: Hindawi Publishing Corporation.
- AL-Zahrani, A. A., Zulkarnain Zainal, Zainal Abidin Talib, Janet Lim Hong Ngee, , Araa Mebdir Holi and Noor Nazihah Bahrudin, (2019) "Effect of the annealing temperature on the photoconversion efficiency of heterostructured photoanode Bi₂S₃/ZnO nanorods in photoelectrochemical cells, special issue of the International Journal of Nanotechnology (Scopus Indexed) by Inderscience Publishers (**In Press**).
- AL-Zahrani, A. A., Zainal, Z., Talib, Z. A., Lim, H. N., & Holi, A. M. (2020). Bismuth sulphide decorated ZnO nanorods heterostructure assembly via controlled SILAR cationic concentration for enhanced photoelectrochemical cells. *Materials Research Express*, 7(2): 025510. (Q2/IF 2019= 1.449). Puplisher: IOP Publishing Ltd.
- Asla.A.AL-Zahrani, Zulkarnain Zainal, Zainal Abidin Talib, Janet Lim Hong Ngee, Laimy Mohd Fudzi, Araa Mebdir Holi and Noor Nazihah Bahrudin (2020) "Enhanced photoelectrochemical performance of Bi₂S₃/Ag₂S/ZnO novel ternary heterostructure nanorods, Arabian Journal of Chemistry, In press. (Q2/IF 2020= 4.7). Publisher: Elsevier.
- Asla.A.AL-Zahrani, Zulkarnain Zainal, Zainal Abidin Talib, Janet Lim Hong Ngee, Laimy Mohd Fudzi, Araa Mebdir Holi and Mahanim Sarif @Mohd Ali (2019) "Effect of the heat treatment on the photoelectrochemical performance of binary heterostructured photoanode Ag₂S/ZnO nanorods in photoelectrochemical cells, Materials Science Forum under the Special Issue «Current Advances in Materials Applications», 1002: 187-199 (Q3/IF 2018= 0.35). Publisher: Trans Tech Publications Ltd.

Asla.A.AL-Zahrani, Zulkarnain Zainal, Zainal Abidin Talib, Janet Lim Hong Ngee, Araa Mebdir Holi (2019) “Bismuth sulphide decorated ZnO nanorods heterostructure assembly via controlled SILAR cationic concentration for enhanced photoelectrochemical cells,” 6th International Conference on Nanotechnology, Nanomaterials & Thin films for Energy Applications(27-29 July 2019). The National Energy University, Kuala Lumpur, Malaysia. (**Best Presenter Award**)

Asla.A.AL-Zahrani, Zulkarnain Zainal, Zainal Abidin Talib, Janet Lim Hong Ngee, Araa Mebdir Holi (2019) “Effect of the annealing temperature on the photoconversion efficiency of heterostructured photoanode $\text{Bi}_2\text{S}_3/\text{ZnO}$ nanorods in photoelectrochemical cells,” International Symposium on Advanced Materials & Nanotechnology (i-SAMN 2019) (19-20th August 2019 at Putrajaya Marriott Hotel, Malaysia.

Asla.A.AL-Zahrani, Zulkarnain Zainal, Zainal Abidin Talib, Janet Lim Hong Ngee, Laimy Mohd Fudzi, Araa Mebdir Holi and Mahanim Sarif @Mohd Ali (2019) “Effect of the heat treatment on the photoelectrochemical performance of binary heterostructured photoanode $\text{Ag}_2\text{S}/\text{ZnO}$ nanorods in photoelectrochemical cells,” 11th International Fundamental Science Congress 2019 (IFSC 2019), 30-31 October 2019, Palm Garden Hotel, IOI Resort City, Putrajaya, Malaysia. (**Best Poster Reward**)



UNIVERSITI PUTRA MALAYSIA

STATUS CONFIRMATION FOR THESIS / PROJECT REPORT

AND COPYRIGHT

ACADEMIC SESSION : First Semester 2020/2021

TITLE OF THESIS / PROJECT REPORT :

SYNTHESIS AND CHARACTERIZATION OF ZINC OXIDE NANORODS SENSITISED BY Bi₂S₃, Ag₂S AND Ag₂S-Bi₂S₃ FOR PHOTOELECTROCHEMICAL APPLICATION

NAME OF STUDENT : ASLA ABDULLAH AL-ZAHRANI

I acknowledge that the copyright and other intellectual property in the thesis/project report belonged to Universiti Putra Malaysia and I agree to allow this thesis/project report to be placed at the library under the following terms:

1. This thesis/project report is the property of Universiti Putra Malaysia.
2. The library of Universiti Putra Malaysia has the right to make copies for educational purposes only.
3. The library of Universiti Putra Malaysia is allowed to make copies of this thesis for academic exchange.

I declare that this thesis is classified as:

*Please tick (✓)

CONFIDENTIAL

(Contain confidential information under Official Secret Act 1972).

RESTRICTED

(Contains restricted information as specified by the organization/institution where research was done).

OPEN ACCESS

I agree that my thesis/project report to be published as hard copy or online open access.

This thesis is submitted for:

PATENT

Embargo from _____ until _____
(date)
(date)

Approved by: